ABSTRACT

Title of Thesis:	OPTIMIZATION IN WIND ENGINEERING USING CYBER-PHYSICAL SYSTEMS FOR THE DESIGN OF PARAPET WALLS
	Michael Lee Whiteman II, Master of Science, 2017
Thesis Directed By:	Assistant Professor, Brian M. Phillips, Department of Civil & Environmental Engineering

Wind-related hazards are becoming an increasing threat as vulnerable coastal locations within the United States continue to see steady population growth. The lack of a corresponding increase in evacuation route capacity means coastal cities will need to rely on shelter-in-place strategies. The significant loss of life and economic impact from windstorms coupled with the expected population increase in vulnerable areas accentuates the need to develop new economical approaches to design and construct buildings capable of surviving extreme wind events. This thesis investigates the use of cyber-physical systems to optimize the structural design of wind-sensitive structures. The proposed design framework combines the efficiency of numerically guided optimization algorithms with the accuracy of boundary layer wind tunnel testing. The focus of this thesis is the development and evaluation of a cyber-

physical approach to wind engineering design and its application to the design of a parapet for a low-rise building.

OPTIMIZATION IN WIND ENGINEERING USING CYBER-PHYSICAL SYSTEMS FOR THE DESIGN OF PARAPET WALLS

by

Michael Lee Whiteman II

Thesis submitted to the Faculty of the Graduate School of the
University of Maryland, College Park, in partial fulfillment
of the requirements for the degree of
Master of Science
2017

Advisory Committee:
Professor Brian M. Phillips, Chair
Professor Bilal M. Ayyub
Dr. Dat Duthinh

Acknowledgements

I would like to express my gratitude to my advisor, Professor Brian M. Phillips for his excellent guidance, expert advice, patience, and support of my academic research for the entirety of my graduate studies at the University of Maryland, College Park. His constant willingness to help, passion in the field, and determination have inspired me.

I would like to thank the efforts of my committee members, Professor Bilal M. Ayyub, and Dr. Dat Duthinh. They have individually and collectively offered excellent feedback, and all of their support and comments are greatly appreciated.

I also would like to thank my friends and family for their support and encouragement. My parents, Kirk Whiteman and Christina Whiteman have been a constant source of love, support, and strength throughout all of these years, and my brother Richard Whiteman has always been willing to help me whenever I have needed his assistance. Finally, I am grateful for the love, encouragement, and tolerance of my fiancée Katie Russell.

This material is based upon work supported by the National Science Foundation under Grant No. 1636039. Any opinions, findings, and conclusions or recommendations expressed in this material are those of the author and do not necessarily reflect the views of the National Science Foundation.

Table of Contents

List of Tables

List of Figures

Chapter 1: Introduction

1.1 Background and Motivation

According to the Population Reference Bureau, the number of deaths from severe weather, tornados, hurricanes, and tropical storms comprises 31.9% of all deaths from natural disasters in the United States from 1970 through 2004 [1]. The National Weather Services reports a combined $529.51M of property damages attributed to thunderstorm wind, tropical storms, and hurricanes in the United States for 2014 and 2015 [2, 3]. Wind-related hazards will become an increasing threat as vulnerable coastal locations within the United States continue to see steady population growth. Furthermore, without a corresponding increase in evacuation route capacity, many coastal cities will have to turn to shelter-in-place strategies. The significant loss of life, economic loss, and expected population increase in vulnerable areas highlights the ongoing need to develop new economical means to deliver buildings which can survive extreme wind events.

Boundary layer wind tunnels (BLWT) remain a leading tool in wind engineering to characterize the pressure loading on wind-sensitive structures. In particular, BLWT testing is valuable when studying new structures for which the simplified provisions of ASCE 7-10 are inadequate or computational fluid dynamics approaches cannot be applied with confidence [4]. While BLWT testing has remained an industry standard for decades, there have been many recent advances in computationally-based optimization techniques for structural design. Meta-heuristic algorithms such as particle swarm and genetic algorithms are problem-independent

algorithms that efficiently explore a complex solution space, providing new opportunities to study multi-variate and multi-objective optimization problems. While new optimization techniques have promise for delivering cost-effective design solutions for wind-sensitive structures, they must be combined with an accurate method such as BLWT testing to evaluate the candidate solutions.

This thesis proposes the use of cyber-physical systems for optimal design in wind engineering. The approach is fully automated, with experiments executed in a BLWT, sensor feedback monitored by a high-performance computer, and optimization techniques used to bring about physical changes to the structural model in the BLWT. Because the model is undergoing physical change as it approaches the optimal solution, this approach is given the name "loop-in-the-model" testing.

The building selected for this study is a low-rise structure with a parapet wall of variable height. Parapets are common on industrial and commercial buildings and help to alleviate extreme roof wind loads [5-8]. Parapet walls alter the location of the roof corner vortex, mitigating the extreme corner and edge suction loads on the roof of the building. Conversely, parapet walls increase the downward roof loads which combine with other roof loads. The influence of parapet height on roof wind loads sets up an interesting optimal structural design problem. The design guidance within ASCE 7-10 is not refined enough in regards to the distribution of parapet loading to determine an optimal parapet height.

In the BLWT, the model parapet height is adjusted automatically using servo-motors to reach a particular candidate design. The building envelope is instrumented with pressure taps to measure the envelope pressure loading. The taps are densely

spaced on the roof to provide sufficient resolution to capture the change in roof corner vortex formation. The taps are uniformly spaced elsewhere to provide necessary resolution to capture the behavior of wind on the remaining structure. Experiments are conducted using a BLWT located at the University of Florida Natural Hazard Engineering Research Infrastructure (NHERI) Experimental Facility.

1.2 Overview of Thesis

The research detailed within this thesis will investigate the use of cyber-physical systems to optimize the structural design of low-rise buildings with parapet walls. The focus of this thesis is the development and evaluation of a cyber-physical approach and its application to determine the optimum parapet height of a building with a predetermined structural frame. The overall goal of this research is to study and improve the accuracy of the optimization process for structures under wind through the use of a BLWT. This proof-of-concept study investigates a single design parameter that has a non-monotonic influence on the performance of a wind-sensitive structure. Implications are significant for more complex structures where the optimal solution may not be obvious and cannot be reasonably determined with traditional experimental or computational methods.

Chapter 2 reviews previous studies on particle swarm optimization and low-rise buildings with parapets. Current knowledge regarding particle swarm optimization is briefly addressed. The current understanding of the effects of wind on low-rise buildings with parapets will be subsequently discussed.

Chapter 3 presents the development of the particle swarm optimization code later applied to wind engineering. A flag variable and fly-back mechanism are

incorporated into the code, and results are obtained for multiple benchmark models. The results for the benchmark models from previous research are then used to validate the improvements to the code.

Chapter 4 describes the geometry and scaling of the model building for the BLWT testing. A description of the materials and components which are used in the model's fabrication are given. The physically adjustable model design variable is presented as well.

Chapter 5 discusses the experimental equipment used for BLWT testing. The method of processing the measured pressure data into the non-dimensional pressure coefficient C_p and the application of the Gumbel distribution to obtain the maximum and minimum C_p values is explained as well.

Chapter 6 presents the preliminary results obtained from the use of a test matrix which consists of a series of tests across angles at 15° increments and parapet heights at 1 inch increments. These results are then analyzed and a comparison is made between BLWT results and ASCE 7-10 provisions.

Chapter 7 describes the setup of parapet design optimization including the problem-specific physical constraints and particle swarm optimization parameters. The structure of the optimization procedure is then presented.

Chapter 8 presents the results of the optimization process based on the static pressure envelope over the roof, inner parapet walls, and the top of the parapet wall. The behavior of all of the particles and their costs over all iterations are presented.

Chapter 9 summarizes the research that is presented in this thesis and presents potential areas for future studies.

Chapter 2: Literature Review

This chapter presents a literature review of particle swarm optimization and the effects of wind on low-rise buildings with parapets.

2.1 Particle Swarm Optimization

Particle swarm optimization (PSO) is a population-based stochastic optimization technique. Particle swarm optimization mimics the social behavior where a population of individuals adapts to its environments by discovering and jointly exploring promising regions. This swarm intelligence method is based on the simulation of social interactions of members of a species, such as the movement of flocks of birds, schools of fish, and swarm of bees. Particle swarm optimization was inspired by evolutionary programming, genetic algorithms, and evolution strategies and shares similarities with genetic algorithms and evolutionary algorithms.

To better illustrate PSO and swarm intelligence, one may imagine a swarm of bees in a field. The goal of these bees is to find the location within the field with the highest density of flowers. Without any previously obtained knowledge, the bees initially begin searching for flowers in random locations with random velocities. As each bee searches the field it can remember the location that it found the highest concentration of flowers, and communicates with other bees to learn the locations where they found highest concentrations of flowers. A bee is attracted both to the location where it had personally found the highest density of flowers and to the location where the swarm as a whole found the highest density of flowers. The bee alters its trajectory to fly somewhere between these two points depending on whether

its decision is dominated by a trust in itself (c_1 in Equation 2.2) or the swarm (c_2 in Equation 2.2). The bee's trajectory is also influenced by its own inertia, that is to say, the bee will continue to some degree along its previous trajectory (w in Equation 2.2). Along the way, the bee might find a location with a higher concentration of flowers than it had previously found. It would then update its memory to be drawn to this new location as well as still being drawn to the location of the most flowers found by the entire swarm. Just as a bee may fly over a place with a concentration of flowers higher than it had personally previously found, a bee may fly over a place with more flowers than had been previously encountered by any bee within the swarm. This would then cause the whole swarm to be drawn toward this new location (in addition to their own personal discoveries). In this manner, the bees will explore the field by flying over locations of greatest concentration and then later being pulled back toward them. The bees are constantly checking the territory that they fly over against their personal locations of greatest concentration (personal best) and the swarm's location of greatest concentration (global best). Eventually, all of the bees swarm around the one place within the field with the highest concentration of flowers. The bees are then unable to find any points of higher flower concentration and are continually drawn back to this location, the swarm's location of greatest flower concentration [9]. This location is taken as the optimal location for harvesting nectar.

Particle swarm optimization is a non-gradient-based, meta-heuristic optimization method [10]. Non-gradient-based optimization techniques are especially useful in solving problems in structural engineering due to their versatility in handling multiple design variables. Particle swarm optimization efficiently explores a large

number of candidate solutions over a large search space without prematurely converging, which can lead to non-intuitive solutions. The technique is easy to program because it is an inherently iterative process reliant on only a few formulas to govern the iterations. Complexities only arise in the analysis of candidate solutions (e.g., in wind engineering) and calculation of the objective function. Also, the problem definition does not require continuity and is capable of handling nonlinear, nonconvex design spaces. In comparison to genetic algorithms there is no mutation calculation; only the best-performing particle transmits information to the others. As a meta-heuristic method, there is no guarantee that a global optimal solution, or even bounded solution will be found [11]. Because the solution is not necessarily optimal, the solution from a PSO algorithm is more precisely termed a sub-optimal solution. Additionally, probabilistic search algorithms tend to require more function evaluations than gradient-based methods to reach an acceptable optimum solution. The technique is also very slow to working out local optimal solutions and may gravitate towards a particle's personal best solution. The technique overall is relatively new so limited studies have been performed related to structural engineering, however research is actively being conducted in order to improve the optimization framework with specific structural engineering considerations.

In the context of structural engineering, the swarm represents a group of candidate design solutions. Each particle within the swarm is a candidate design which consists of an N-dimensional finite position and velocity. The position refers to the values of N design parameters (e.g., cross-sectional areas of the members) while the velocity refers to the changes in the design parameters from one iteration to the

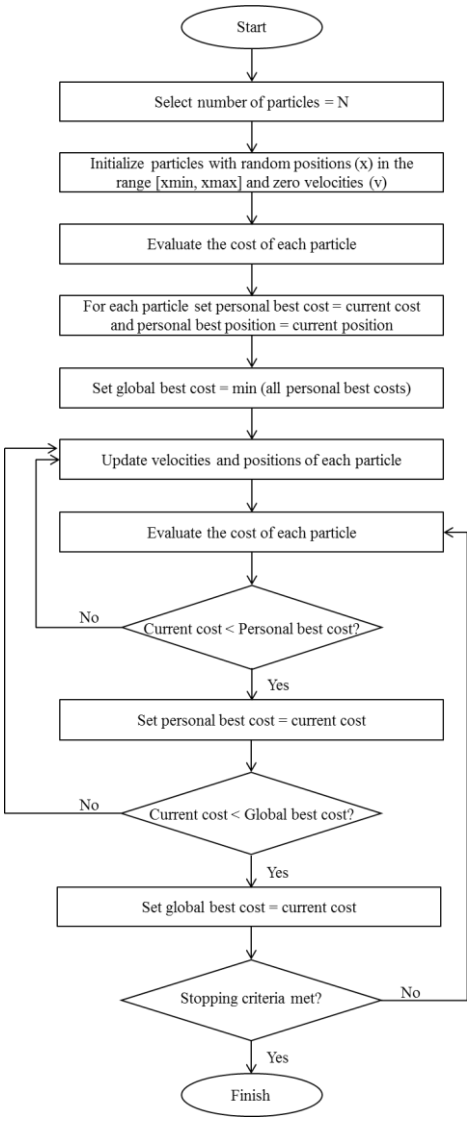

Figure 2.1 Outline of a basic particle swarm optimization algorithm

next. The position of the particles is often initially randomly distributed throughout the design space. These candidate solutions then iteratively move throughout the search space seeking better positions are found with the expectation that the swarm of particles will move toward the best solutions. This process is repeated either for a predetermined number of design iterations, or until convergence is reached. An outline of a basic PSO algorithm is given in Figure 2.1.

The process for updating the position of each particle is

$$x_{j+1}^{i} = x_{j}^{i} + v_{j+1}^{i}\Delta t \tag{2.1}$$

where x_{j+1}^{i} is the position of particle i at iteration $j+1$, v_{j+1}^{i} is the corresponding velocity vector of the particle, and Δt is the time step value.

The procedure for determining the velocity vector of each particle in the swarm depends on the particular PSO algorithm. The process which is commonly used for updating the velocity vector was first introduced by Shi and Eberhart as

$$v_{j+1}^{i} = wv_{j}^{i} + c_1 r_1 \frac{\left(p_j^i - x_j^i\right)}{\Delta t} + c_2 r_2 \frac{\left(p_j^g - x_j^i\right)}{\Delta t} \tag{2.2}$$

where r_1 and r_2 are independent random numbers in the range [0,1], p_j^i is the best known position of particle i considering iterations 1 through j, p_j^g is the best known position of all particles considering iterations 1 through j, and Δt is the time step value [12]. Throughout the present work a unit time step of one iteration is used. An alternative method for determining p_j^g is to use the best position of all particles only considering the current iteration [13]. In Equation 2.2, there are three problem-dependent parameters that influence every particle's velocity: the inertia of the particle, w and two trust parameters, c_1 and c_2. The inertia controls the algorithm's exploration properties; a larger inertia enables a more global search of the design space because particles are more inclined to continue on their previous trajectory. The trust parameters indicate how much confidence the current particle has in itself, c_1 and in the swarm, c_2 and will draw the particle to these respective best positions. When PSO was originally introduced, Kennedy and Eberhart proposed that c_1 = c_2 = 2 in order to give the products of $c_1 r_1$ and $c_2 r_2$ each a mean of 1 [14]. Shi and

Eberhart analyzed the difference in performance and accuracy for both fixed and time-decreasing inertia weights. Based on empirical studies, an inertia weight of $w = 0.8$ was the only fixed inertia weight to never fail in finding an acceptable solution regardless of velocity limits. A time-decreasing inertia weight from 1.4 to 0 was found to be better than a fixed inertia weight; the larger initial inertia weight enables a broad global search while the smaller final inertia weight forces more local searches [15]. Shi and Eberhart conclude that it is best to use a fixed inertia weight of $w = 0.8$ or $w = 1.0$ dependent upon the selection of the values of the velocity limits, and that a time varying inertia weight would result in an even better performance. Ultimately, the selection of inertia and trust weights are problem dependent and their values must be determined case-by-case. A poor selection of parameters may lead to premature convergence to a solution that is not globally optimal, or at the other extreme, a solution that takes an excessive number of iterations to converge. Parameter selection can be done through trial and error or through deduction and personal judgment.

To increase the performance and accuracy of PSO, multiple enhancements to the standard algorithm have been proposed and tested. The first of these enhancements is the inclusion of convergence criterion within the problem statement. The purpose of proper convergence criterion is to ensure that the optimization process avoids unnecessary calculations once an optimum solution is reached. Preferably the convergence criterion should be general (i.e., not include parameters that are specific to the problem). One common practice is to assume that convergence is obtained if the change in the objective function is below a particular threshold for a specified number of iterations [16]. Basic PSO is for unconstrained problems only, and original

literature for basic PSO does not address particles which violate design constraints. Thus, constrained optimization has been introduced which usually addresses this problem through the use of different methods including penalty functions, a fly-back mechanism, or resetting the particle velocity to zero.

A penalty function penalizes the objective function when one or more constraints are violated. If penalty coefficients are used, but appropriate coefficients cannot be provided, then difficulties will be encountered. Additionally, penalty functions reduce the overall efficiency of the PSO; it resets infeasible particles to their previous best positions, sometimes preventing the search from reaching global max.

Another method for addressing particles which violate design constraints involves the use of a "fly-back mechanism" which is able to accelerate the convergence rate and improve the accuracy effectively in comparison with the PSOPC and basic PSO algorithms respectively. With the use of a fly-back mechanism, if it is determined that a particle would violate the position constraints of the design space, then the direction of the particle's velocity is reversed and the position is recalculated for the particle so that it will reach its original position. The global minima of design problems have been found to usually be close to the boundaries of the feasible search space. By enforcing a particle to return to its original position and assuming that the global best particle remains in the same position, then the direction of the velocity in the next iteration will still point to the boundary but will point closer to the global best particle [17].

Another method involves resetting particle i's velocity to zero if it violates one or more constraints at iteration j. The velocity vector for particle i at iteration $j+1$ would then be given as

$$v_{j+1}^{i} = c_1 r_1 \frac{\left(p_j^i - x_j^i\right)}{\Delta t} + c_2 r_2 \frac{\left(p_j^g - x_j^i\right)}{\Delta t} \tag{2.3}$$

Therefore, the velocity of particle i at iteration $j+1$ would only be influenced by the best known position of particle i considering iterations 1 through j, and the best known position of all particles considering iterations 1 through j. This would remove all influence of the particle's current trajectory and would likely cause the particle to return to the feasible design space in the next iterations [7].

2.2 Effects of Wind on Low-Rise Buildings with Parapets

Parapet walls are typically low-rise walls constructed along the perimeter of a roof. These walls act as guard rails, prevent fires traveling up exterior walls from reaching the roof surface, and also reduce suction loads on the roof surface. With regard to wind loading, parapet walls alter the location of the roof corner vortex, mitigating the extreme corner and edge suction loads on the roof of the building. Most current research on parapet walls focuses on the local pressure distribution of roofs with parapets, as in components and cladding, and on using parapet with non-uniform or modified geometries in an effort to reduce the overall magnitude of wind-induced loading. These studies use a BLWT to capture the complex and turbulent wind flows around the parapet [5]. Additionally, a few studies consider the effect of parapets on the underlying structural members [6, 18].

Recent studies on the effects of parapets on flat rooftops on low-rise buildings have uncovered inconsistencies with previous research [5, 6, and 19]. These inconsistencies are the result of an insufficiently dense region of static pressure taps in the upwind corner of the roof of the model which caused the true peak suction pressure values to not be measured [19]. Thus, it is essential to have a very high density of static pressure taps in the upwind corner region to ensure that the peak suction pressures are appropriately obtained.

It is well known that for wind at oblique angles to a building with flat rooftop's walls that strong vortices occur near the upwind corner [19]. These vortices, similar to the vortex that is produced at the leading edge of delta type wings and as such are also known as delta wing vortices, create an area of high suction on the surface of the roof near the corner [20]. Solid, continuous perimetric parapets taller than 1 m act to reduce both the mean and peak pressure coefficients in the corner region of these buildings. Most building codes, such as ASCE 7-10, allow for some method of pressure reduction over different regions of the roof for the presence of parapets, however there has not been extensive research conducted regarding accurate regions of reduction based upon the geometry of the building and parapet or on the optimal height of a parapet for a given low-rise building [4]. Additionally, research has primarily focused on the corner zones of roofs with limited research focusing on the edge and interior zones. The research regarding the edge and interior zones has mainly focused on mitigating local loading through the use of alternative geometries and not much in regards to the effect of different heights of solid, perimetric parapets or on the optimal height of solid, perimetric parapets [8].

2.3 Chapter Summary

This chapter reviews a number of previous studies on PSO and on the effects of wind on low-rise buildings with parapets. Particle swarm optimization has been demonstrated as an effective procedure to obtain the optimal solution to a particular objective without the need for a gradient and while considering multiple constraints. Previous studies on parapet walls do not thoroughly discuss edge and interior zones on the roofs of low-rise buildings with parapets or the optimal height of solid, perimetric parapets on low-rise buildings. This research will provide guidance, through the use of a BLWT, to the parameters that constitute optimal parapet design.

Chapter 3: Background

This chapter presents the development of an introductory particle swarm optimization code in MATLAB [21]. The code is then validated by a comparison with the results of multiple benchmark models.

3.1 Code Development

The standard particle swarm optimization (PSO) algorithm as described by Figure 2.1 was initially adopted and taken from pseudo-code to a MATLAB script. The details of this flow chart were discussed in Chapter 2.

For a series of initial studies, the PSO algorithm will be applied to the design of steel truss systems. The objective of the steel truss systems is to minimize the total weight of the truss. The *N*-dimensional position of an individual particles is the set of *N* element cross-sectional areas that create a candidate truss design solution. The possible particle positions components are taken from an allowable range of cross-sectional areas. A constraint is added such that members cannot exceed their yield stress.

Subsequent studies applied the PSO algorithm to the design of a steel frame system. The objective of the steel frame systems is to minimize the total weight of the frame. The *N*-dimensional position of the particles within the swarm are the *N* member selection of the beams and columns. The possible particle positions are taken from the discrete set of steel W-shape member sizes for all AISC W-shape member sizes from W4x13 to W36x652 with all relevant member properties. Constraints are based on the strength and serviceability requirements are taken from the American

Institute of Steel Construction (AISC) Steel Construction Manual [22]. Constraints include design strengths for axial loading, strong-axis bending, and weak-axis bending were determined based upon Chapters D, E, and F from the AISC Steel Construction Manual. The interaction of axial loading and flexure for doubly symmetric members is determined based upon Chapter H. The effective length method was used for the design of all beam-columns within the structure. The effective length factor, K was calculated for a frame with sidesway uninhibited (moment frame) using equation C-A-7-2 from the AISC Steel Construction Manual.

Recalling the analogy of PSO to a swarm of bees within a field from Chapter 2, each bee would correspond to a candidate solution for both the truss and frame systems. The position of a bee within the field would correspond to a set of element cross-sectional areas for the truss systems or a set of ASIC W-shape members for the frame systems. The total weight of the truss or frame for the truss and frame systems, respectively would correspond inversely to the concentration of flowers at the bee's location; the lower the total weight the higher the concentration of flowers. The bees will then eventually swarm around one particular position which obtains the highest concentration of flowers, corresponding to the set of element cross-sectional areas or set of AISC W-shape members which obtains the lowest total weight of the truss or frame systems respectively.

A finite element analysis code was written in MATLAB to analyze the candidate design solutions. Member properties, topology, and orientation were used to develop a global stiffness matrix for candidate design. Loads were applied directly to the nodes of the structure and a linear-elastic first-order analysis was performed.

From the solved nodal deformations, member-level axial forces and flexural moments were calculated to compare with strength and serviceability constraints. The strong-axis and weak-axis internal moments for the member were calculated using the second derivative of the element shape functions.

Multiple enhancements were made to the standard PSO algorithm to increase the computational efficiency and decrease the overall run time of the algorithm. A fly-back mechanism was incorporated to keep particles within their design space constraints. If the position of the particle was found to be outside of the feasible range of particle positions, then the position of the particle was recalculated using the particle's negative velocity, effectively returning to its previous position. Additionally, a Boolean flag variable was introduced for all particles. This variable was triggered if a particular particle for the current iteration violated any strength, serviceability, or problem-specific design constraints. If a particle were to become flagged, the code would skip subsequent constraint checks. Only particles that satisfied all constraints were considered when calculating the objective function of total structural weight and updating personal and global best costs. This standard PSO algorithm with multiple modifications is outlined in Figure 3.1.

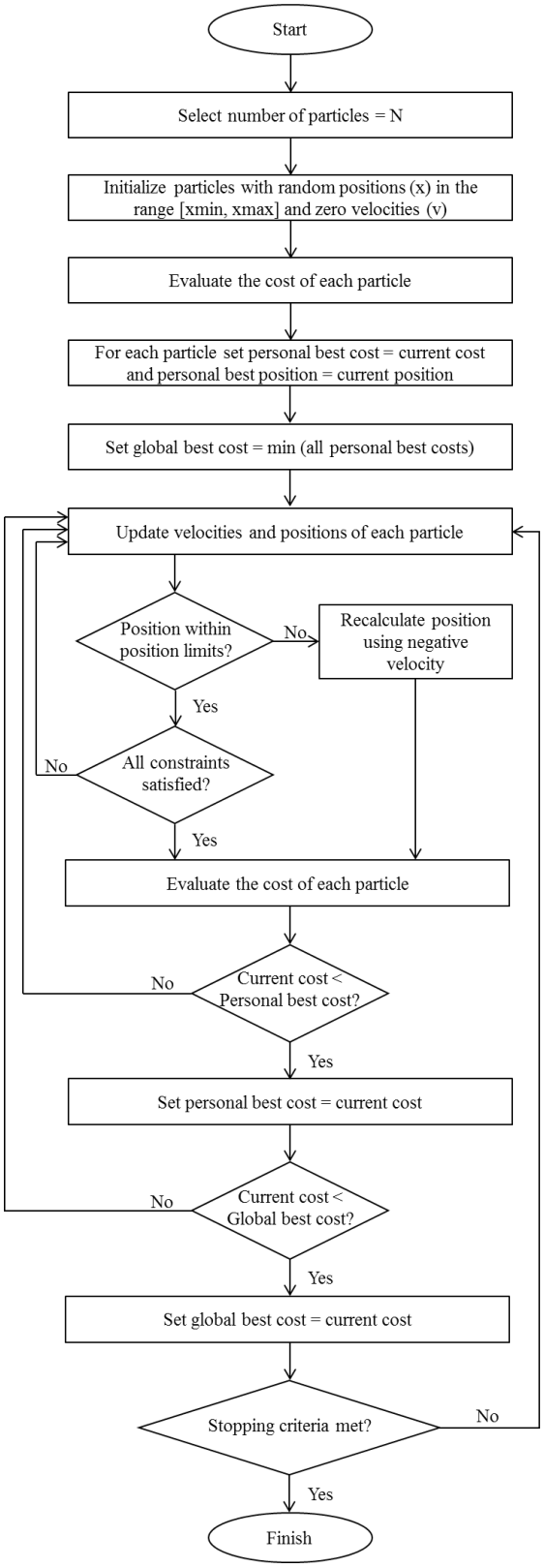

Figure 3.1 Particle swarm optimization code with modifications

3.2 Benchmark Models as Validation

The modified PSO algorithm was validated by a comparison with the results of multiple established benchmark models and the results of previous research.

The 10-bar truss structure, shown in Figure 3.2, has previously been analyzed by multiple researchers [23]. All necessary problem parameters are expressed in Table 3.1; σ_{allow} is the maximum axial stress that is allowed to be applied on any of the structural members and d_{allow} is the maximum nodal displacement that is allowed in the vertical or horizontal direction. For this benchmark problem, the initial enhancement of a flag variable was included in the PSO algorithm. A study was then conducted on the benefits of (1) a fly-back mechanism and (2) a linearly-decreasing inertia weight. In all, four cases were created as summarized in Table 3.2.

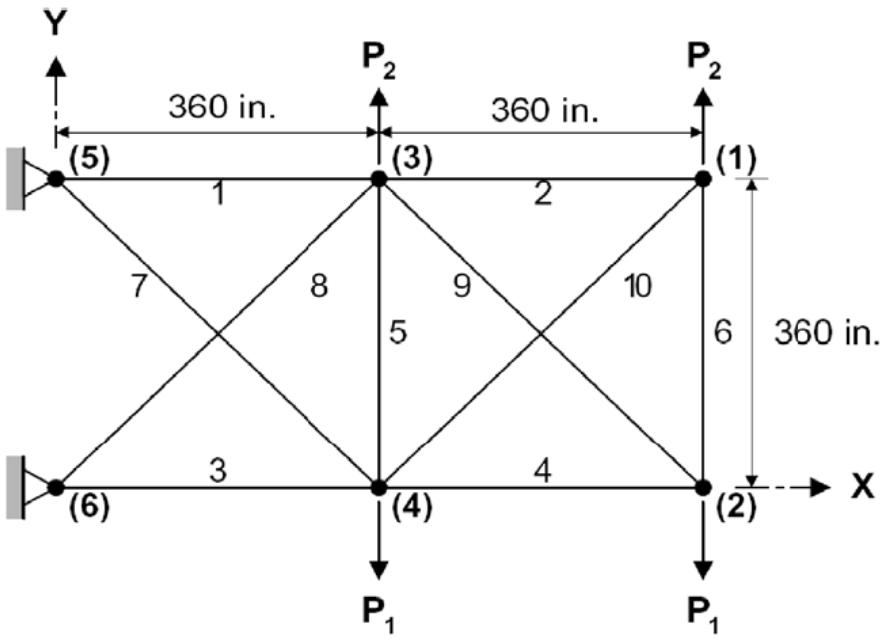

Figure 3.2 A 10-bar planar truss structure

Table 3.1 Parameters for the 10-bar planar truss structure

Problem Parameters			
Design Parameters	**Value**	**PSO Parameters**	**Value**
Material density (lb/in^3)	0.1	Number of particles	50
Modulus of elasticity (ksi)	10,000	w	Varies
σ_{allow} (ksi)	±25	c_1	0.8
d_{allow} (in)	±2.0	c_2	0.8
P_1, P_2 (kip)	100, 0	Max Iterations	3,000

The modified PSO algorithm was run 50 times for each of the four cases. The constant inertia weight and linearly decreasing weight cases which include the fly-back mechanism display faster convergence rates than the constant inertia weight case without a fly-back mechanism, and slower convergence rates than the linearly decreasing inertia weight case without a fly-back mechanism. For all cases, a minimum weight was determined to be approximately 5,070 lbs. However, both cases which include the fly-back mechanism determined an optimal solution that was an average of 150 lbs. lighter than the cases without the mechanism. Table 3.2 shows a summary of the results from the 50 optimization runs for each case. The fly-back mechanism performed better than simple position limits as seen in the lower costs on average. There was very little difference between the average weight for the constant inertia weight and linearly decreasing inertia weight cases with a fly-back mechanism. Although these observations may be problem-specific, a constant inertia weight will be used for all subsequent PSO algorithms due to the simplicity and

consistency regardless of the number of maximum iterations. Table 3.3 shows the solution for the case of a constant inertia weight and fly-back mechanism compared to those of previous researchers.

Table 3.2 Comparison of inertia weights and fly-back mechanism for the 10-bar planar truss (a) optimal weight and (b) number of iterations to obtain the optimal weight

(a)

Weight (lb)				
Condition	**Only Position Limits**		**Fly-back Mechanism**	
	Constant w =0.9	**Linearly Decreasing w = 0.9 to 0.4**	**Constant w =0.9**	**Linearly Decreasing w = 0.9 to 0.4**
Minimum	5077.50	5065.06	5065.06	5070.90
Maximum	6856.80	6863.70	6328.70	6443.80
Average	5328.37	5448.54	5237.53	5234.60
Std. Deviation	382.36	465.27	288.40	282.71

(b)

Iteration Number to Reach Best Cost				
Condition	**Only Position Limits**		**Fly-back Mechanism**	
	Constant w =0.9	**Linearly Decreasing w = 0.9 to 0.4**	**Constant w =0.9**	**Linearly Decreasing w = 0.9 to 0.4**
Minimum	125.0	1.0	200.0	150.0
Maximum	2800.0	1400.0	2100.0	2100.0
Average	797.5	398.0	572.0	522.5
Std. Deviation	613.1	249.6	317.9	361.7

Table 3.3 Comparison of solutions for 10-bar planar truss

Optimal Cross-Sectional Areas ($in.^2$)							
Bar Areas	**Schmit [24]**	**Rizzi [25]**	**Lee [26]**	**Li, PSO [23]**	**Li, PSOPC [23]**	**Li, HPSO [23]**	**Current**
A_1	33.430	30.730	30.150	33.469	30.569	30.704	31.532
A_2	0.100	0.100	0.102	0.110	0.100	0.100	0.101
A_3	24.260	23.930	22.710	23.177	22.974	23.167	22.903
A_4	14.260	14.730	15.270	15.475	15.148	15.183	15.424
A_5	0.100	0.100	0.102	3.649	0.100	0.100	0.101
A_6	0.100	0.100	0.544	0.116	0.547	0.551	0.666
A_7	8.388	8.542	7.541	8.328	7.493	7.460	7.403
A_8	20.740	20.950	21.560	23.340	21.159	20.978	20.202
A_9	19.690	21.840	21.450	23.010	21.556	21.508	21.771
A_{10}	0.100	0.100	0.100	0.190	0.100	0.100	0.100
Weight (lb)	5089.0	5076.7	5057.9	5529.5	5061.0	5060.9	5065.06

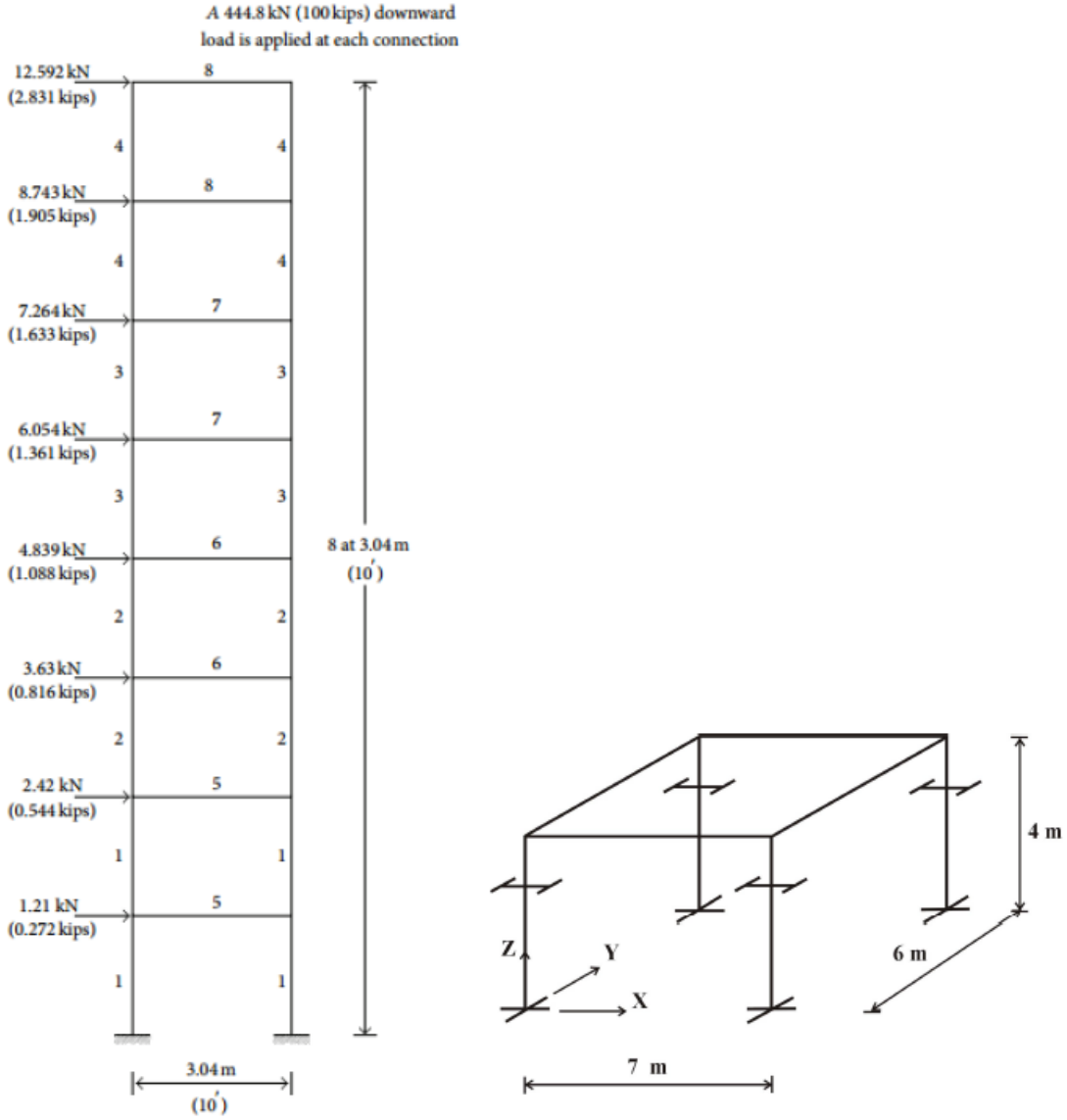

Figure 3.3 Topology of 1-bay 8-story frame and 1-story 8-member space frame

Two additional benchmark structures were considered to develop and verify additional PSO features. The 1-bay 8-story frame and the 1-story 8-member space frame are both shown in Figure 3.3. These two structures are both frames, requiring axial and flexural interaction equations for strength checks and the use of a discrete

lookup table for possible steel member shapes. The 1-bay 8-story frame was considered to study the grouping of members constrained to have the same steel shape, a common practical design consideration. The 1-story 8-member space frame was incorporated to extend the PSO algorithm from 2-dimensions to 3-dimensions to include different member rolls (orientation about the longitudinal axis) and a stiffness matrix for 3-dimensional frame elements. To quickly visualize the results, the PSO code included the plotting of the deflected shape, visualization of the values of the axial-flexural interaction equation using a color bar, and plotting the best cost of the population of particles across all iterations. Examples of these for the 1-bay 8-story frame can be seen in Figures 3.4, 3.5, and 3.6, respectively.

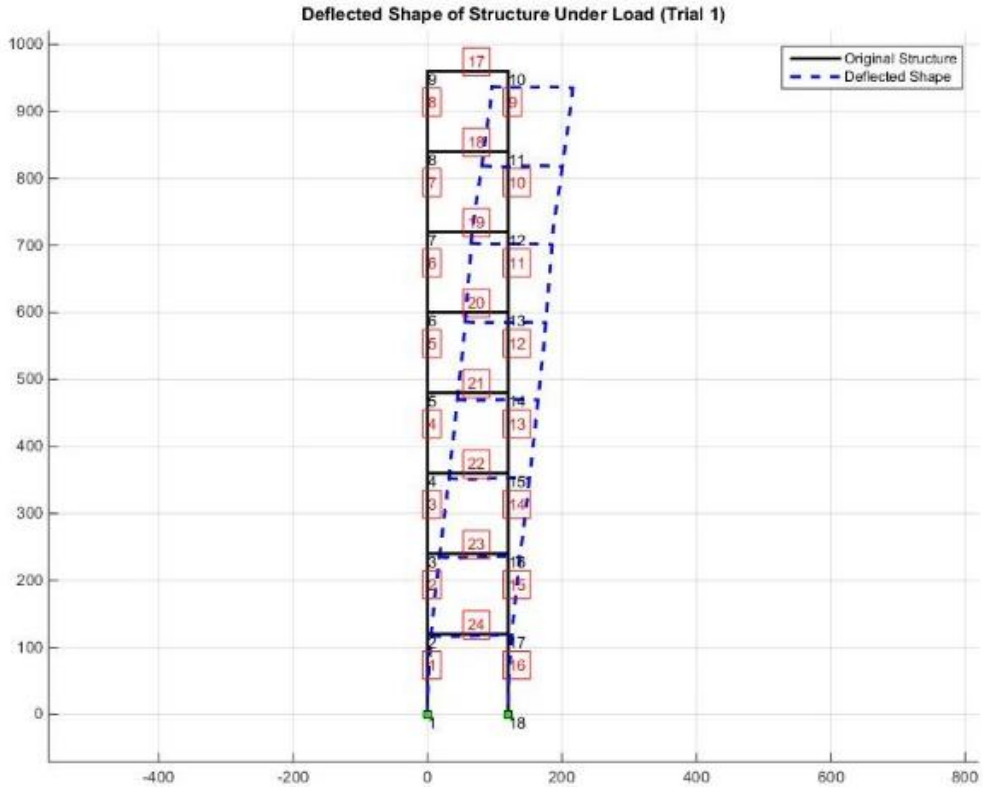

Figure 3.4 Sample deflected shape of 1-bay 8-story frame

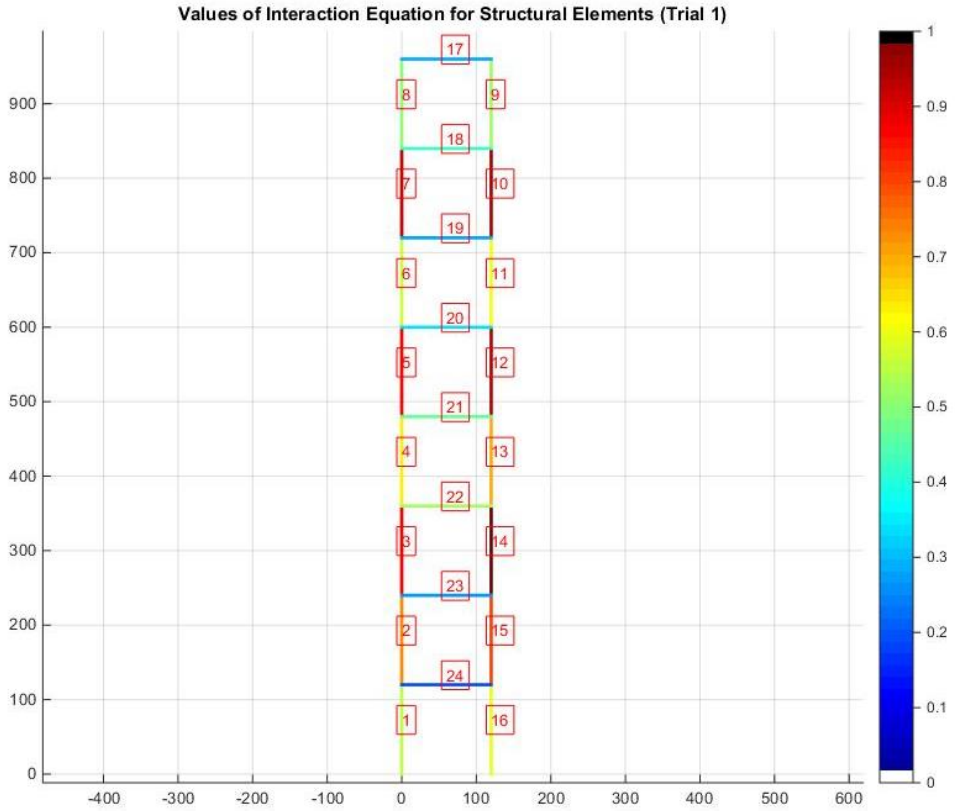

Figure 3.5 Sample interaction equation heatmap of 1-bay 8-story frame

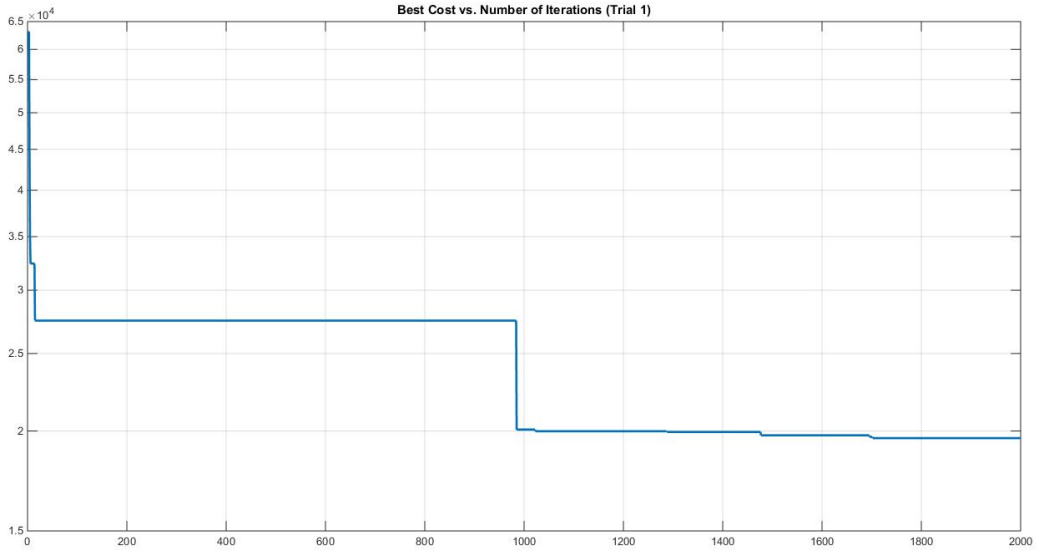

Figure 3.6 Sample best cost vs. number of iterations of 1-bay 8-story frame

3.3 Chapter Summary

This chapter describes the benchmark models that were used to develop a PSO approach capable of optimizing structural design problems subject to the LRFD design requirements as per the AISC Steel Construction Manual. First, a ten-bar planar truss structure is presented. The dimensions and design properties of this structure are given, as well as the solutions for the optimal design of this structure obtained by previous research. The optimal solution achieved compares very well to that of multiple previous researchers. The topology of two other models, a 1-bay 8-story frame, and 1-story 8-member space frame, are presented. These models are used to incorporate practical aspects design for frame structures. The results of these frame structures are not presented in detail as there are no enhancements to the algorithm made, only the extension of its functionality.

Chapter 4: Model Development

This chapter presents the details of the model low-rise building with a structural parapet. The scale, dimensions, and materials are given. The selection and creation of a physically adjustable design variable for the model building is also presented.

The model is created for evaluation using a boundary layer wind tunnel (BLWT), the leading experimental tool in wind engineering to characterize the pressure loading on a structure. One fundamental type of structure that can be modeled and evaluated through BLWT testing is a rigid model. Rigid models offer a simple testing approach that is sufficient for structures that have little aerodynamic damping, such as low-rise buildings. The model created for this study is assumed rigid.

4.1 Physically Adjustable Design Variable

This thesis focuses on a proof-of-concept for a cyber-physical systems approach to the optimization of wind-sensitive structures. Numerically derived candidate solutions must be physically recreated in the BLWT such that their envelope wind loads are accurately measured. A single controllable design variable is sufficient to demonstrate the cyber-physical approach to optimization. Additionally, by limiting the study to a single design variable, unnecessary mechanical complexity is avoided and focus is instead placed on the optimization framework.

The variable chosen is the parapet wall height of a low-rise building. The parapet wall will be actuated by four linear motors, one at each corner of the model.

The inner core of the model remains stationary, maintaining a constant building height with variable parapet. Strips made from Teflon PTFE were used between the inner core and parapet walls to assist in achieving smooth linear actuation. A foam gasket was used between the outer parapet walls and the wooden turntable to allow for the parapet wall to linearly actuate but prevent any air pressure from leaking around the model after actuation and during testing. The performance of the gasket is explored in Chaper 5.

4.2 Model Geometry

The low-rise building with a parapet is modeled after a two-story office building. When selecting the building scale, the physical limitations of the BLWT and BLWT turntable must be considered. The BLWT turntable allows the model to rotate and experience different wind approach angles. The model and parapet actuation system must all fit within the 40 inch diameter turntable. For this to occur, the diagonal of the model in plan is desired to be less than 36 inches. Additionally, a length to width ratio of 1.5 is desired to have a rectangular model building. This leads to the model dimensions of 29.25 inches × 19.50 inches, with a diagonal of 35.15 inches. To represent a low-rise building, a model height of 20 inches is selected.

Additionally, urethane tubing will be installed on the outer and inner sides of the parapet to measure the wind pressures on both sides. This requires a total thickness of the model parapet walls of at least 1 inch to accommodate the thickness of polycarbonate sheets, tubulation (metal ends of the urethane tubing), and minimum bend radius of 0.5 inches for the 0.063 inch urethane tubing. The static pressure taps

on the outer and inner parapet walls are staggered to permit a thinner model parapet wall.

Based on the physical model dimensions and the target two-story office building, a model to full-scale ratio of 1:18 was selected. This results in a building with full-scale dimensions of 29.625 feet × 44.4375 feet in plan, 30 feet tall, and a parapet that is 1.5 feet thick. According to the Building Code Requirements for Masonry Structures, parapet walls should have a thickness of at least 8 inches [27]. The building model represents a realistic two-story full-scale building with a two by three bay steel frame. The fully-constructed model is depicted in Figures 4.1, 4.2, and 4.3.

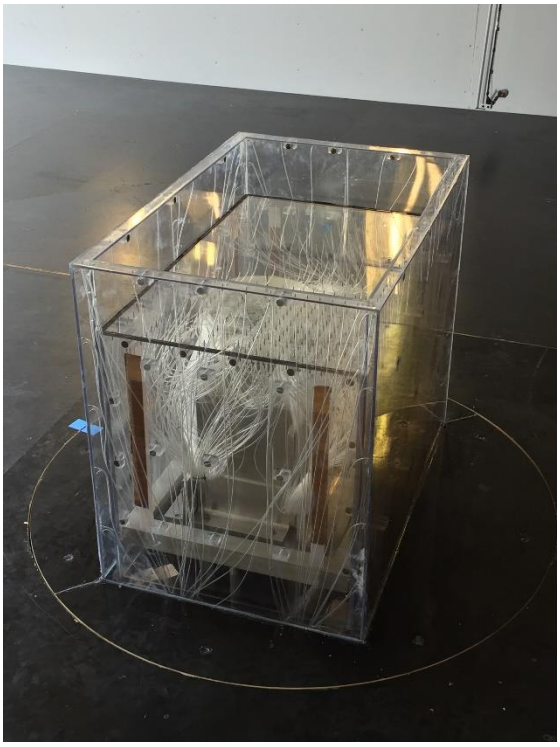

Figure 4.1 Isometric view of parapet model

Figure 4.2 Roof and top of parapet of parapet model

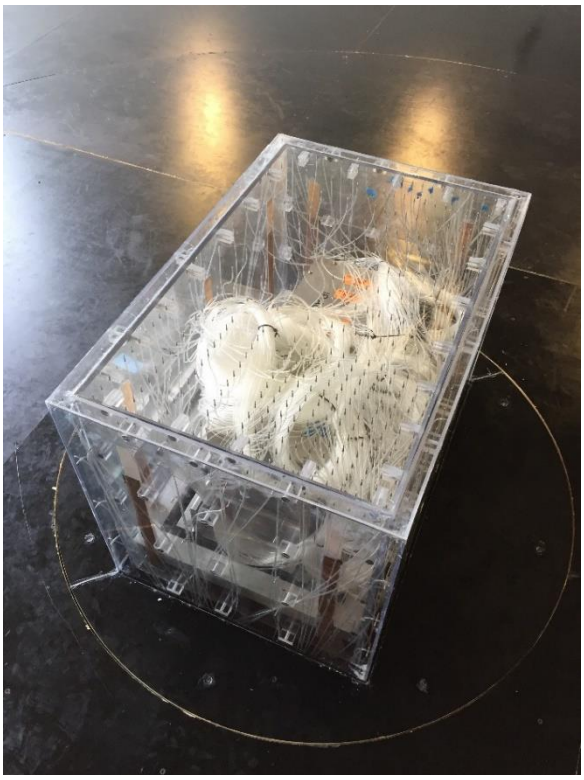

Figure 4.3 Dense corner region of roof

4.3 Materials

Clear, impact-resistant polycarbonate is selected for all building surfaces as it remains rigid against the expected pressures in the BLWT. Additionally, it is easier to machine than other clear plastics. The nominal thickness of the polycarbonate sheets was selected as small as possible to avoid an excessively thick parapet wall, while still providing enough rigidity to prevent flexure of the walls. The nominal thickness of the polycarbonate sheets for the parapet walls was selected to be 0.1875 inches. To increase the rigidity of the parapet structure, 0.625 inch thick polycarbonate blocks with screws were used to connect the outer and inner parapet wall panels. The inner core of the model was only exposed to the flow of wind through the roof. The nominal thickness of the polycarbonate sheets used to manufacture the inner core was selected to be 0.25 inches. The separate outer and inner model sections are shown in Figure 4.4. There are two layers of polycarbonate for the parapet wall (outer model section), and the inner core (inner model section) is a box with an open bottom.

Figure 4.4 Parapet model separated in sections: parapet wall (outer model section, left) and inner core (inner model section, right)

To capture the envelope wind pressure, 0.054 inch I.D. urethane tubing was used with 0.063 inch O.D. stainless steel tubulation; the urethane tubing was stretched to securely fit around the tubulation. This tubulation was then inserted into 0.0625 inch diameter holes that were drilled into sheets of polycarbonate.

The linear actuation of the parapet wall structure around the inner core of the model was achieved through the use of Nanotec LS4118S14004-T6x1-150 linear actuators, as depicted in Figure 4.5.

Figure 4.5 Nanotec LS4118S14004 linear actuator

These motors were connected to the parapet walls through the use of polycarbonate triangular supports as depicted in Figure 4.6.

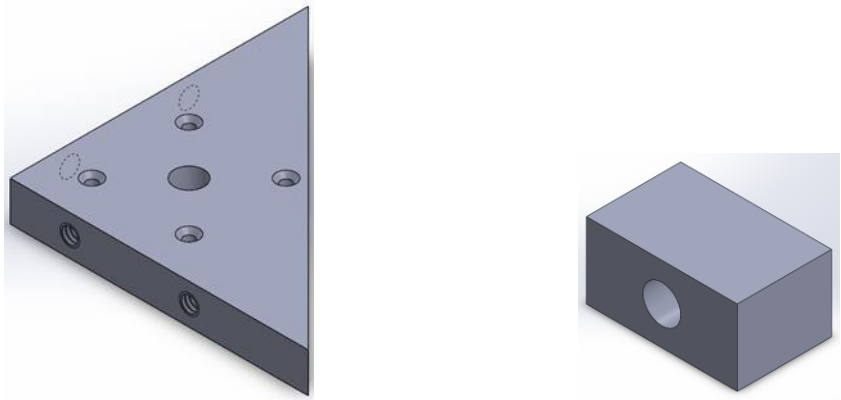

Figure 4.6 Polycarbonate triangular support and polycarbonate blocks

The motors were attached to the triangular supports using screws, which were then connected to the parapet walls through the use of polycarbonate blocks similar to those used for increased rigidity, as seen in Figure 4.6. The drive shafts of the linear actuators were housed inside of a 6.5 inch round base plate and steel pipe within a 7" PVC pipe. The PVC pipe was placed on the outside of the drive shaft of the linear actuator in order to protect the shaft from coming into contact with any urethane tubing during actuation while testing as seen in Figure 4.7.

Figure 4.7 Linear actuator with PVC shield

4.4 Chapter Summary

The parameters of the model are presented in this chapter in detail, including the design variable, model topology, and materials utilized. The reasoning for the choice of parameters is presented as well. The model is fabricated from polycarbonate

so that it can withstand the forces and stresses induced under testing conditions, and uses a combination of polycarbonate blocks to increase rigidity. The thickness of the parapet is 1 inch with a full-scale thickness of 18 inches to represent a realistic parapet and allow for full-scale dimensions similar to a low-rise building.

Chapter 5: Experimental Setup and Data Processing

This chapter discusses the experimental equipment that is used to conduct the experiment. The method of converting raw pressure data into a non-dimensional pressure coefficient, C_p is discussed as well.

5.1 Experimental Equipment

The optimization framework is run from a coordinating computer which both runs the MATLAB optimization algorithms and interfaces with other electronic components. This computer controls the boundary layer wind tunnel (BLWT) turntable angle and the linear motors which adjust the parapet height of the model. The coordinating computer allows the entire testing procedure and all modifications to the model and testing environment to be executed autonomously.

The pressure on the building surfaces within the BLWT is measured using Scanivalve ZOC33 pressure scanners. The ZOC33 pressure scanners have 64 pressure inputs. A total of 8 ZOC33 scanners were available, resulting in a maximum of 512 static pressure taps.

Experiments are conducted using a BLWT located at the University of Florida Natural Hazard Engineering Research Infrastructure (NHERI) Experimental Facility. The BLWT is 6.1 m wide with a 1 m turntable centered along the 6.1 m width 31.75 m downwind of 8 fans. The fans are consistently kept at 1050 RPM for all testing, which corresponds to a reference height velocity of approximately 14 m/s. The BLWT contains a terraformer field in-between the fans and test section which can

adjust the terrain roughness. For the tests herein, an open terrain condition was created. The BLWT with the parapet model installed is depicted in Figure 5.1.

Figure 5.1 Boundary layer wind tunnel with parapet model, upwind view

To ensure that the measured pressure represents realisting building conditions, there had to be no leaking of pressure within or around the model. The performance of the Teflon and model construction were tested through the use of a plastic drum; the plastic drum was placed around the model and a seal between the plastic drum was formed. A constant supply pressure was then input into the drum, and the air pressure measured from Scanivalve was monitored for any large changes over time. A relatively constant pressure was measured for all Scanivalve channels, and the model was therefore deemed to not have any internal pressure leaks. The performance of the foam gasket was tested through the analysis of multiple scenarios: no gasket, only the foam gasket, and the foam gasket sealed with silicone, hereafter called “fully

sealed". The pressure measured by a select subset of taps was compared for the different scenarios, and the difference in measured pressure between only the foam gasket and the fully sealed case was determined to be minimal. Therefore, the case of only the foam gasket was selected as it obtained pressure measurements similar to the fully sealed case, and elminates the need to consistently reapply the silicone seal for each parapet height.

5.2 Tap Tributary Areas

The tributary area of a tap encompasses the area on which the measured pressure is assumed to act. The tap locations are known based upon their surface number, spacing, and the parapet height at any given time. Tap tributary areas are calculated using Voronoi diagrams, which are derived from Delaunay triangulation. For a given set of points (taps) Delaunay triangulation created triangles that: (1) do not overlap, (2) cover the entire interior space formed by the points, and (3) do not have any points within the triangle's circumcircle. A corresponding Voronoi diagram is created by drawing perpendicular bisectors to the sides of the triangles. Regions formed by these bisectors contain one point each and bound an area that is closer to that point (tap) than to any other point. This automated method to calculate tap tributary areas is particularly important because the geometry of the building changes with every model.

Figures 5.2 and 5.3 shows the tributary areas of all of the acceptable static pressure taps for parapets of 1 inch and 5 inches respectively. The center surfaces are the roof and the top of the parapet wall. The outer and inner parapet walls are then folded out from one another in such a manner that they are connected where they

would connect with the top of the parapet wall. As the parapet height increases, the tributary areas for both the outer and inner parapet walls increase as well. The irregular tributary areas seen on a few wall surfaces are due to some channels on the Scanivalve system reporting unrealistic pressure time histories.

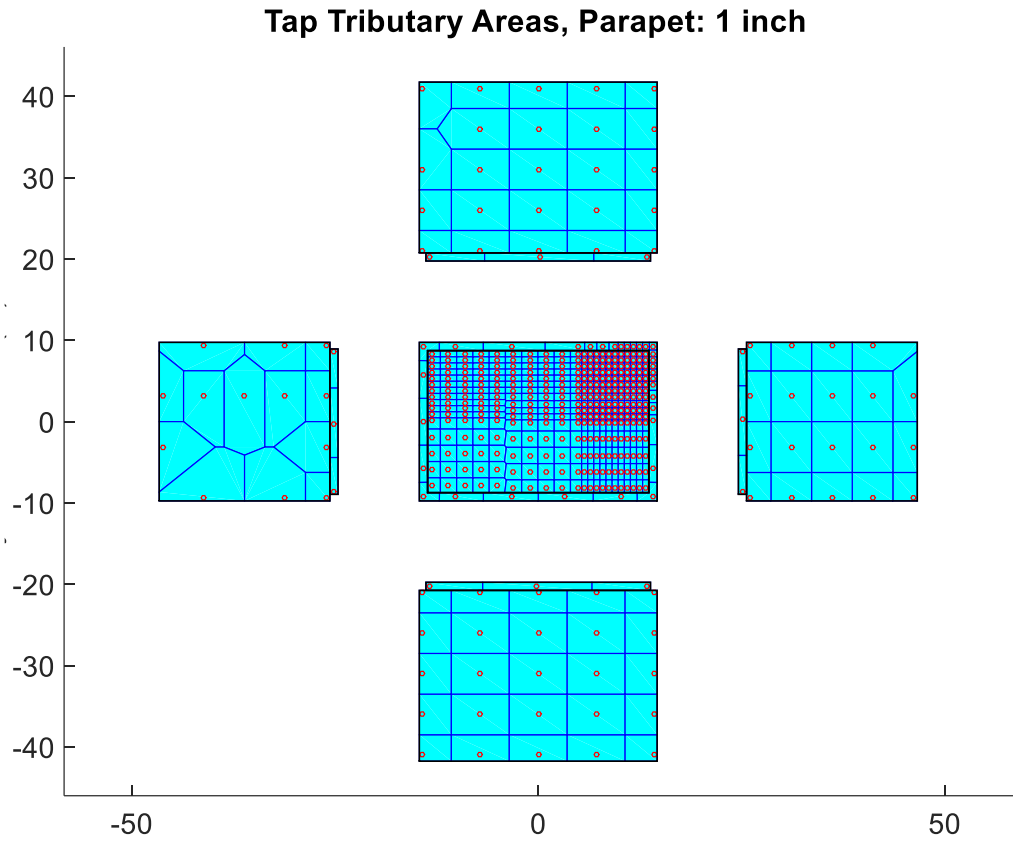

Figure 5.2 Tap tributary areas for a parapet of 1 inch

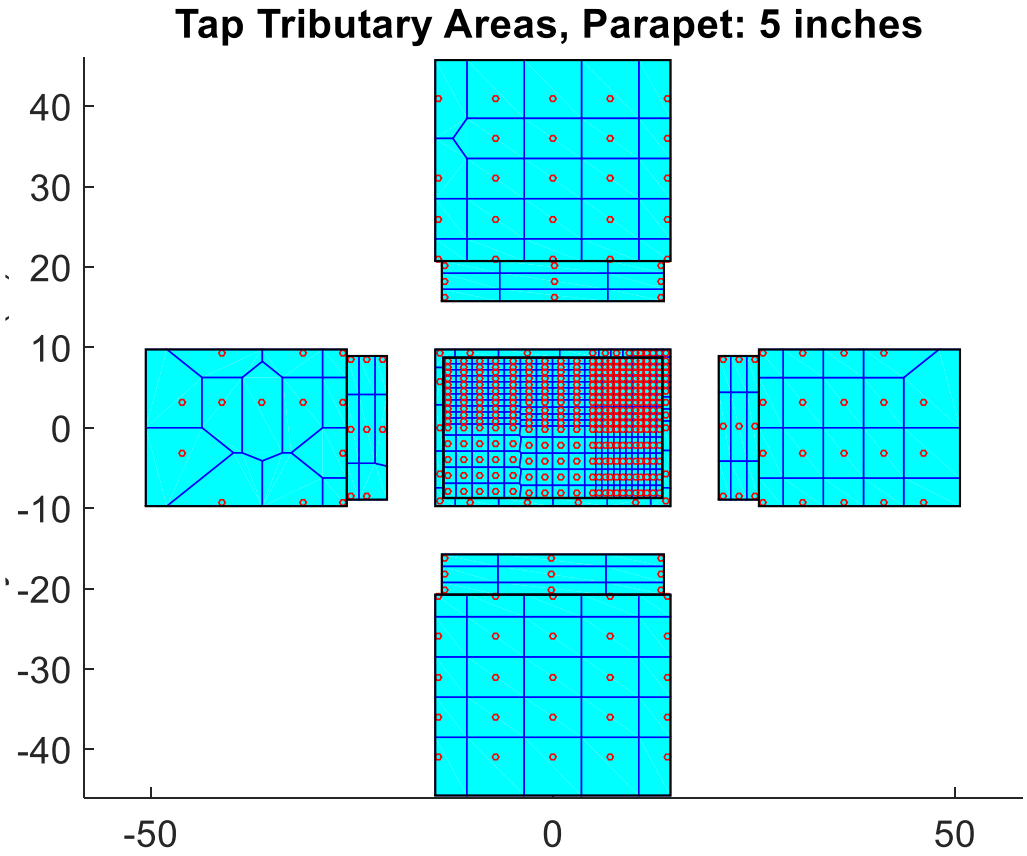

Figure 5.3 Tap tributary areas for a parapet of 5 inches

5.3 Assessment of Pressure Coefficients

The pressures at all static pressure taps were measured simultaneously and sampled at a sampling rate of 625 Hz. Data is collected for two minutes in model scale, corresponding to approximately 11 minutes full scale assuming a basic wind speed of 40 m/s. For each test the non-dimensional pressure coefficient, C_p, was calculated using the equation

$$C_p = \frac{(p - p_0)'_M}{\frac{1}{2}\rho U_{ref}^2 R_h^2} \tag{5.1}$$

where p is the wind pressure on the surface of the model measured by Scanivalve, p_0 is the static pressure at the reference height, and ρ is the air density. The reference height for all tests is taken to be the eave height of the building model. In order to estimate this value, a reference wind speed measurement, U_{ref} is obtained from pitot tubes above the boundary layer. This reference wind speed measurement is then converted to a mean wind speed at the eave height through a conversion factor, R_h. The sign of the pressure coefficient indicates the direction of the wind pressure on the surface of the model; a positive value indicates wind pressure acting towards the surface while a negative value indicates away from the surface. The C_p values are based on the model-scale velocity and test duration. The C_p values could be normalized differently for comparison with ASCE 7-10 values, however this was not necessary for the scope of the work herein.

The maximum and minimum pressure coefficients were estimated for each wind attack angle using a Gumbel distribution. The Gumbel distribution fitting method is a commonly used method for estimating peak pressures on low-rise buildings. The measured model-scale record of C_p is truncated into 50 segments of equal length. The peak maximum and minimum pressure coefficients from each segment are then taken, and the 78th percentile is then used to estimate the maximum and minimum C_p values. The method used to fit the Gumbel distribution is a linear polynomial curve which is solved using the method of linear least squares.

5.4 Chapter Summary

The experimental equipment used for experimental testing is described, including Scanivalve ZOC33 pressure scanners and the BLWT. Then the process for

determining the tributary areas of the static pressure taps using Voronoi diagrams is described. The method of processing the measured pressure data into the non-dimensional pressure coefficient, C_p, and using the Gumbel distribution to obtain the maximum and minimum C_p values are discussed as well.

Chapter 6: Preliminary Results

This chapter presents preliminary results in the form of a test matrix. The test matrix includes a comprehensive set of wind approach angles and parapet heights. These results are then compared qualitatively to ASCE 7-10 parapet provisions.

6.1 Test Matrix

A test matrix was obtained by testing all wind approach angles from 0° to 360° by 15° increments with 0° indicating the broad side of the building with the dense roof taps facing upwind. Parapet heights from 0 inches to 5 inches were tested for 2 minutes for each wind approach angle at increments of 1 inch. Data was obtained from the boundary layer wind tunnel (BLWT) test using the Scanivalve pressure scanner. The test matrix served to validate that all of the channels in use were returning reasonable data as expected. In particular, because the building is double symmetric and evaluated from 0° to 360°, it was straightforward to identify taps that were returning inaccurate data. A few taps were found to be "bad" and eliminated from future data processing.

The purpose of the test matrix was also to obtain training data to develop a better understanding of the behavior of the air flow across the roof for a low-rise building with different parapet heights. This allowed for the development of a realistic objective function for the optimization of the parapet height in consideration of the static envelope while providing the opportunity to compare the results with those that would be expected using ASCE 7-10.

6.2 Benefits and Drawbacks of a Parapet

An increasing parapet height reduces the minimum pressure on the roof. As the height of the parapet increases, the minimum C_p on the roof surface decreases. This decrease is best observed under the angle of 45°. Figures 6.1, 6.2, and 6.3 demonstrate the decreasing C_p measured on the surface of the roof for 45°.

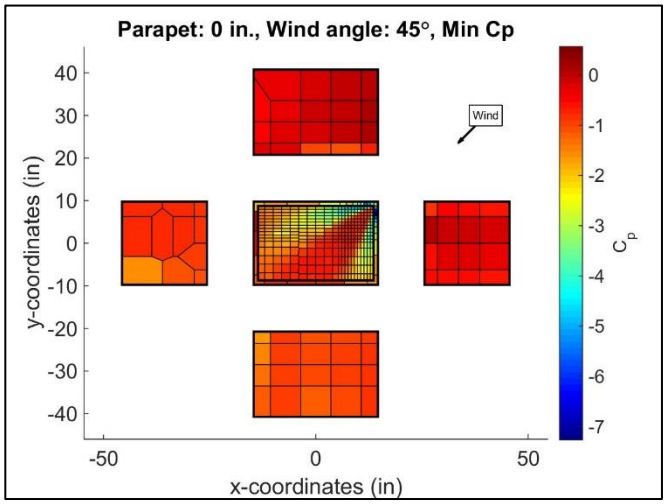

Figure 6.1 Minimum C_p for no parapet at an angle of 45°

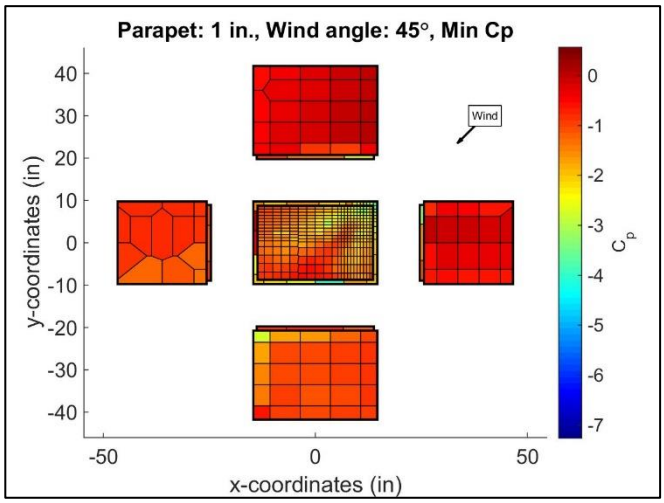

Figure 6.2 Minimum C_p for a parapet of 1 inch at an angle of 45°

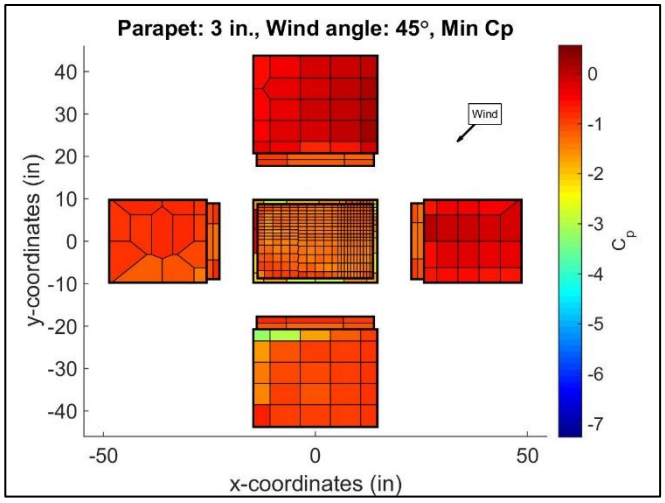

Figure 6.3 Minimum C_p for a parapet of 3 inches at an angle of 45°

An increasing parapet height, however, increases the suction on the inner parapet wall surfaces. This increase is best observed under the angle of 90°. Figures 6.4, 6.5, and 6.6 demonstrate the increasing minimum C_p measured on the inner parapet wall surfaces for 90°.

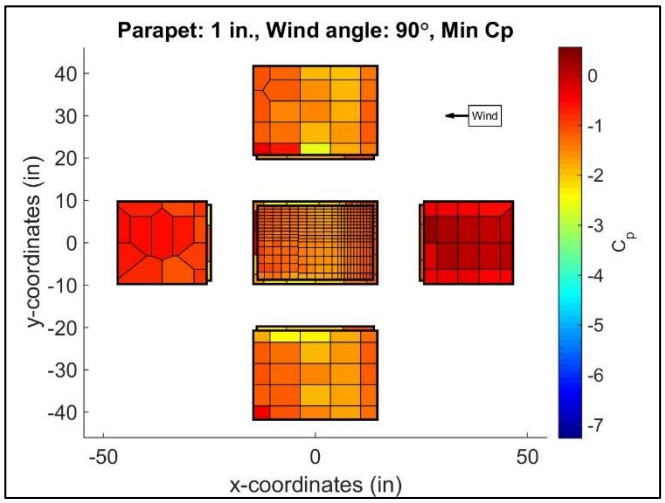

Figure 6.4 Minimum C_p for a parapet of 1 inch at an angle of 90°

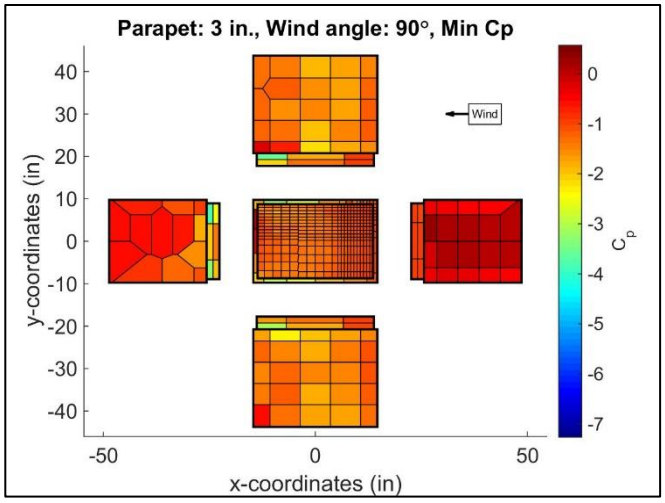

Figure 6.5 Minimum C_p for a parapet of 3 inches at an angle of 90°

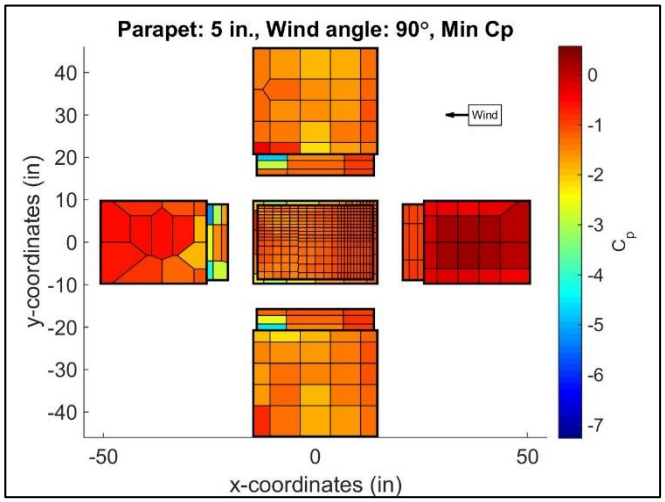

Figure 6.6 Minimum C_p for a parapet of 5 inches at an angle of 90°

As the parapet height increases, the decreasing minimum C_p on the roof and increasing minimum C_p on the inner parapet wall represents a tradeoff that can be translated into a simple optimization problem.

6.3 Comparison of Results with ASCE 7-10

Recalling Chapter 5, the C_p values obtained are not normalized to a gust of any particular duration length. Therefore, any conclusions made from comparisons

between the obtained C_p values and those expected from ASCE 7-10 are based upon the direction of expected wind pressure and not the magnitude.

According to ASCE 7-10 Section 27.6.2 for the determination of the main wind-force resisting system wind loads on parapets, the C_p of the external and internal parapet walls are expected to be opposite in sign as depicted in Figure 6.7 [4]. ASCE 7-10 assumes that there is no shielding, and therefore there should be no reduction on the positive wall pressure on the inner side of the leeward parapet. Additionally, the roof is expected to experience a suction across its entire length that decreases in magnitude.

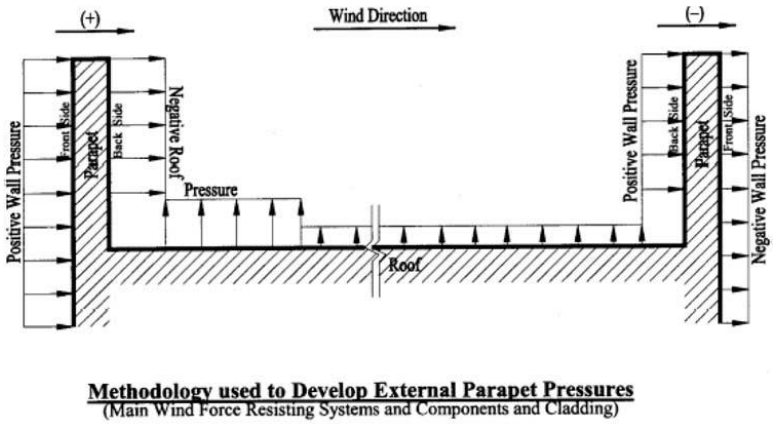

Figure 6.7 External parapet pressures on the outer and inner parapet walls as per ASCE 7-10 [4]

Figures 6.8, 6.9, 6.10, and 6.11 show the maximum C_p of all surfaces of the building at the angle of 0° for model scale parapet heights of 1 inch and 5 inches. For a parapet height of 1 inch, the windward wall side has a positive maximum C_p on the outer parapet wall and a negative maximum C_p on the inner parapet wall, consistent with Figure 6.7 from ASCE 7-10. Focusing on the inner parapet wall of the leeward

side, the outer regions have a positive maximum C_p while the inner region has a negative maximum C_p. This indicates that the inner region of the inner parapet wall experiences suction on the entire time. This unexpected behavior is further supported with the taller parapet of 5 inches. The expected direction of pressure (consistent with ASCE 7-10) is only experienced for the windward wall and at the top of the inner parapet wall at the downwind corners. These results are consistent for all heights at 0°. This suggests that with the presence of taller parapets the windward parapet will reduce the positive wall pressure to the leeward parapet through shielding.

Figures 6.12, 6.13, 6.14, and 6.15 show the maximum C_p of all surfaces of the building at the angle of 90° for model scale parapet heights of 1 inch and 5 inches. For a parapet height of 1 inch, the edge of the roof along the back surface of the leeward parapet has a positive maximum C_p value. This unexpected behavior is supported with the taller parapet of 5 inches; there is an increasing value of positive maximum C_p along the back surface of the leeward parapet wall. This behavior is best observed under the wind angle of 90°. This suggests a buildup of pressure along the back surface of the leeward parapet wall that develops over the length of the roof.

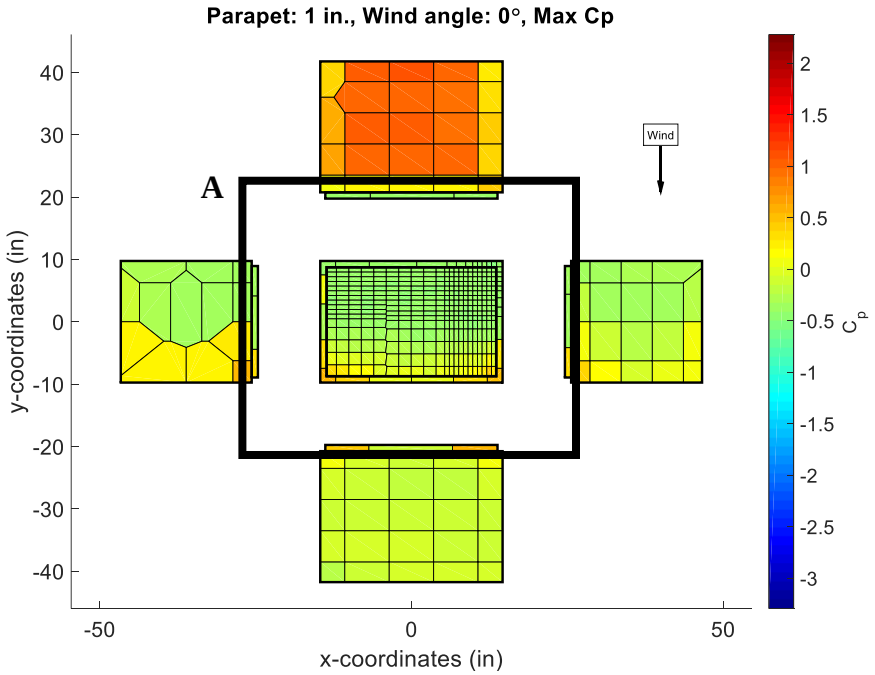

Figure 6.8 Maximum C_p of all surfaces for a 1 inch parapet at an angle of 0°

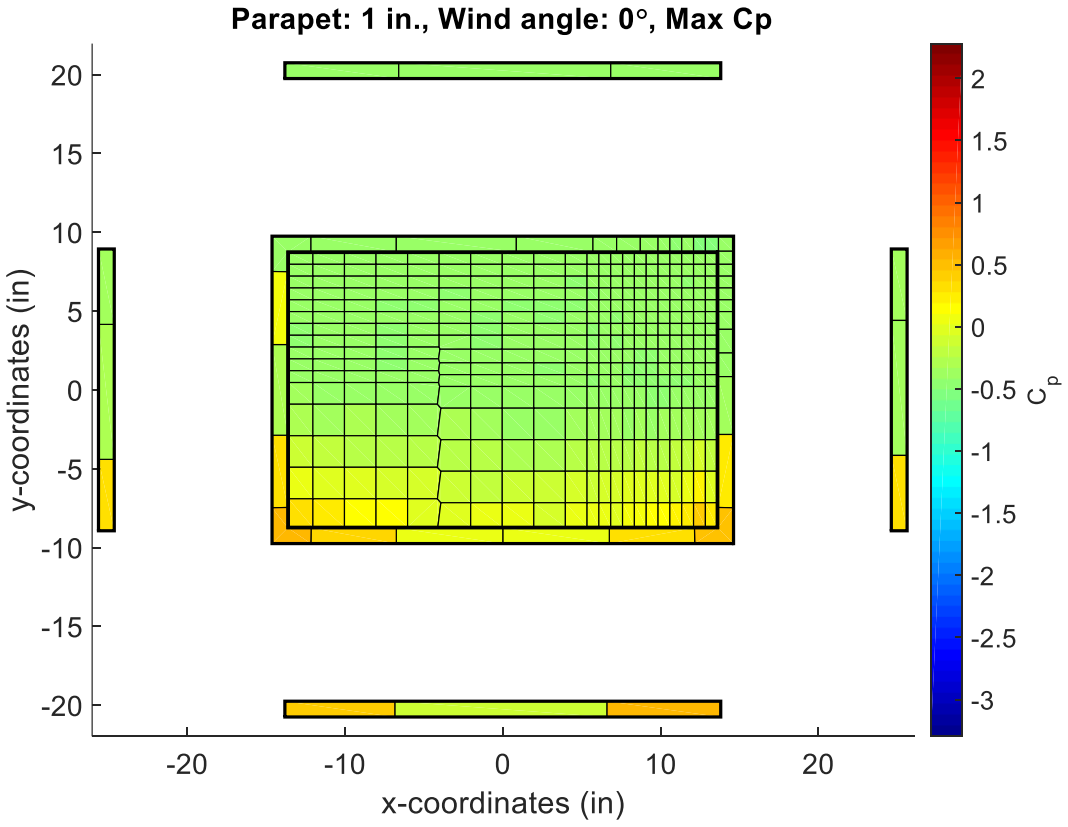

Figure 6.9 Surface A of Figure 6.8

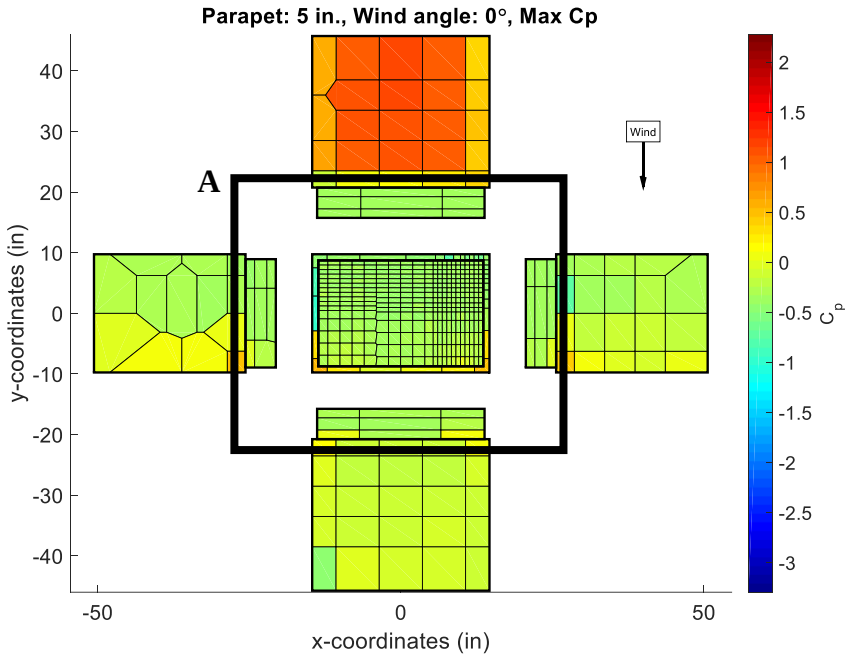

Figure 6.10 Maximum C_p for all surfaces for a 5 inch parapet at an angle of 0°

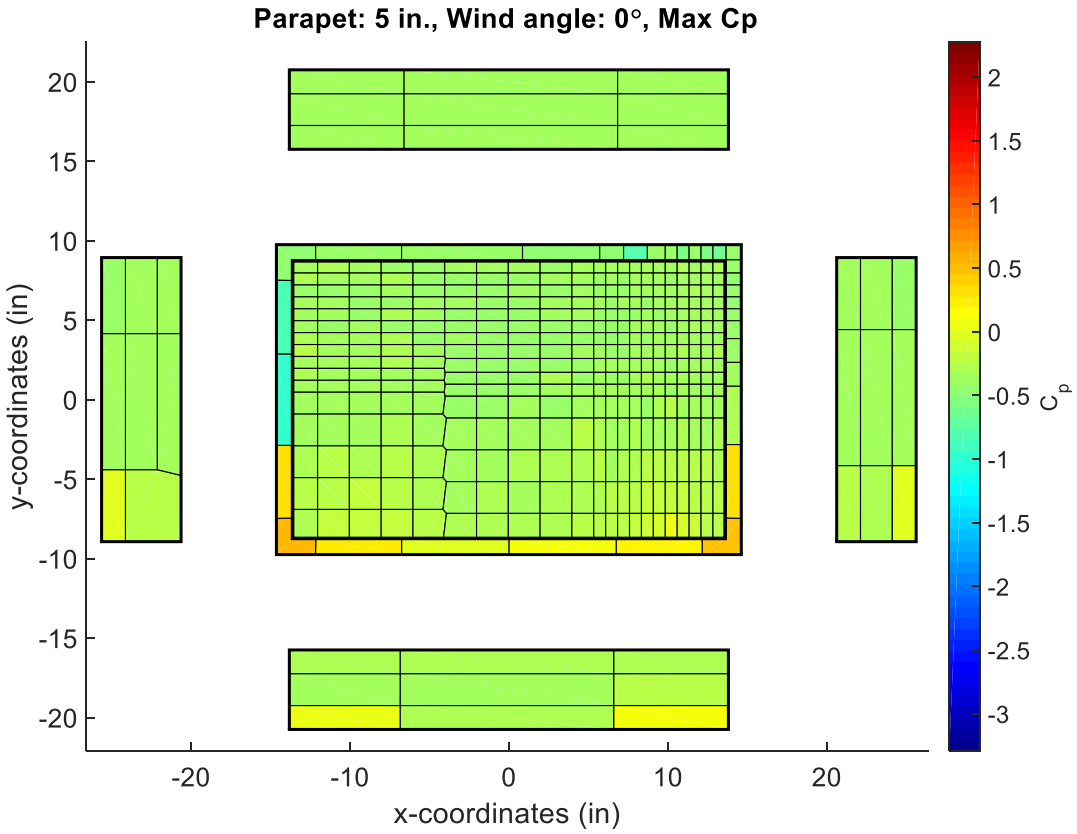

Figure 6.11 Surface A of Figure 6.10

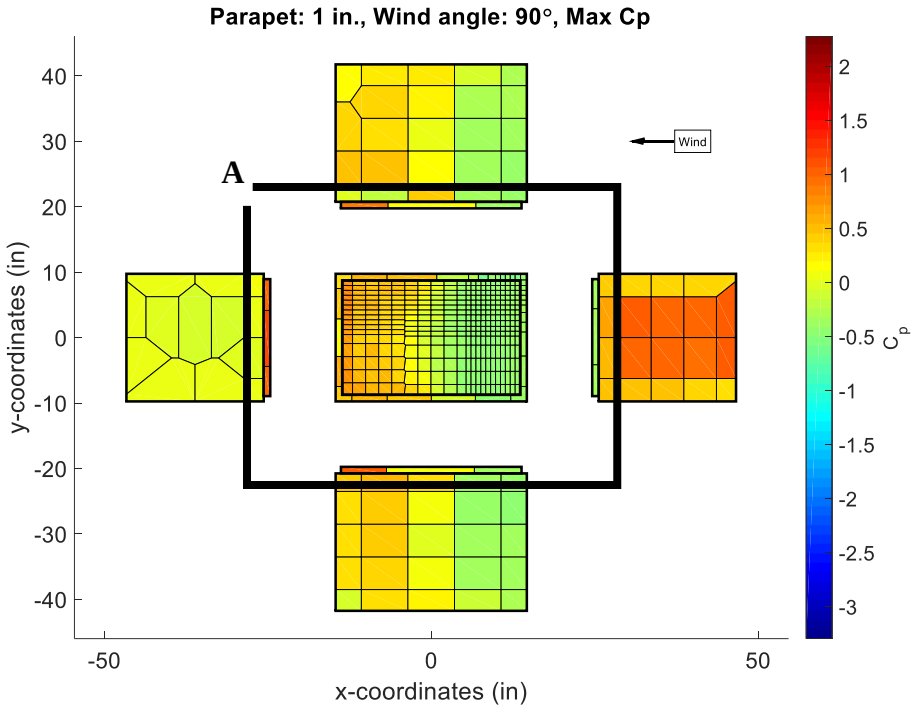

Figure 6.12 Maximum C_p for all surfaces for a 1 inch parapet at an angle of 0°

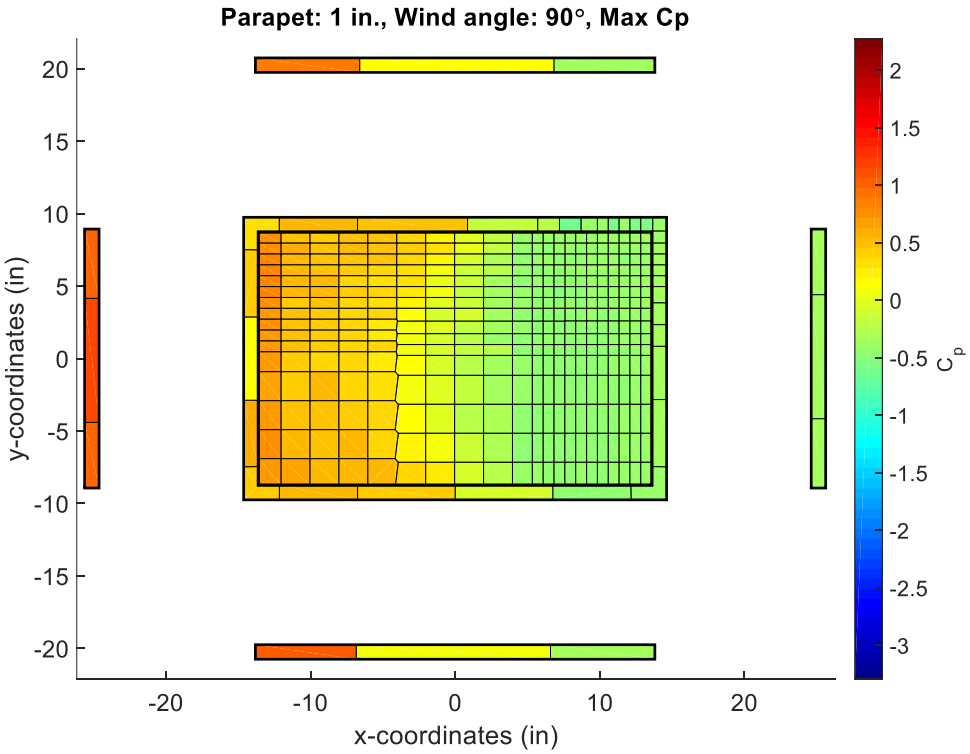

Figure 6.13 Surface A of Figure 6.12

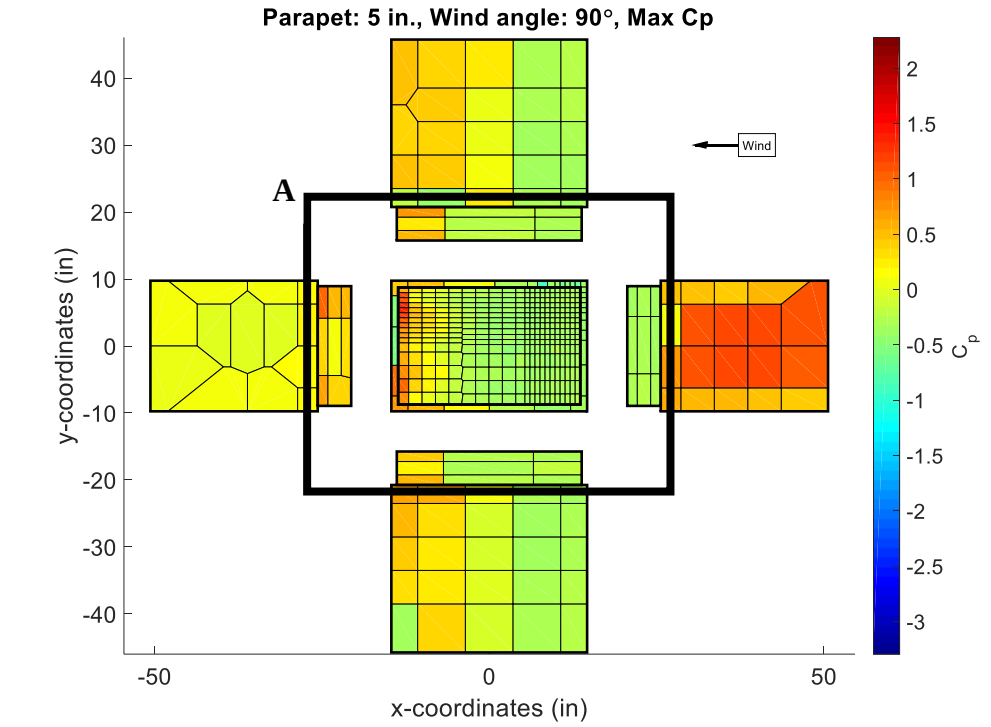

Figure 6.14 Maximum C_p for all surfaces for a 5 inch parapet at an angle of 0°

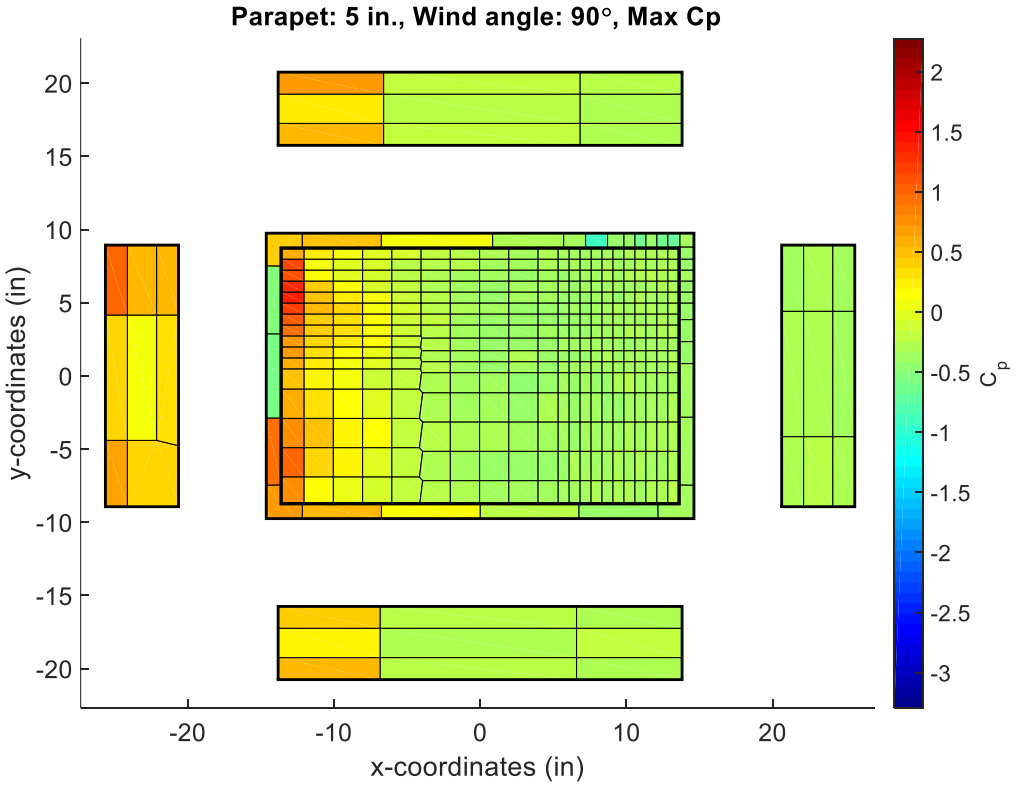

Figure 6.15 Surface A of Figure 6.14

6.3 Chapter Summary

The preliminary results obtained are presented in this chapter in detail, including the explanation of the test matrix. These results are then compared to those expected from using ASCE 7-10 as well. The purpose of the test was matrix was to verify that all channels being used were returning data as expected, and to develop a better understanding of the air flow across the building for different parapet heights. This would allow for a more realistic objective function to be developed for the optimization in consideration of the static envelope. The results for the direction of wind on the inner parapet walls were different compared to the results with those that would be expected using ASCE 7-10. The assumed wind directions in ASCE 7-10 may not encompass the worst case scenarios. Future work will explore these observations is more detail.

Chapter 7: Optimization Framework

This chapter presents the optimization problem setup, including the specific objective, constraints, and parameters. The objective function for the optimization problem is to minimize suction on the roof, inner parapet walls, and top of the parapet wall subject to the constraint that the parapet height remain between 0 and 4.5 inches in model scale.

7.1 Problem Setup

The optimization problem was constrained physically by the maximum achievable parapet height of 4.5 inches in model scale. This limit was enforced in the optimization algorithm to avoid motor controls which would produce displacements larger than 4.5 inches.

Recalling the analogy of PSO to a swarm of bees within a field from Chapter 2, each bee would represent a potential design solution for the parapet optimization. The position of a bee within the field would correspond to a particular model scale parapet height. The maximum suction measured on the roof, inner parapet wall, and top of the parapet wall surfaces would correspond inversely to the concentration of flowers at the bee's location; the lower the maximum suction the higher concentration of flowers. The bees will then eventually swarm around one particular position which obtains the highest concentration of flowers, corresponding to the height which obtains the lowest maximum suction on the roof, inner parapet wall, and top of the parapet wall surfaces.

The problem-specific particle swarm optimization (PSO) parameters of $w, c_1,$ and c_2 were selected to be equal in magnitude so that an equal weight would be placed on the particle's inertia, trust in itself, and trust in the particle swarm. Due to the relatively small domain for position it was important to ensure that the particles remained within the feasible design space. Therefore, after initial testing the magnitude of 0.5 was assigned to all problem-specific parameters. Considering the time limits on experimental resources, a balance was achieved between sufficient particles to create a swarm effect in PSO and sufficient iterations to see convergence. Based on an estimated two minutes per BLWT run, one minute to set up the BLWT run, and a day of testing, the number of particles was selected to be five.

The building model has an axis of symmetry across both axes in the transverse plane, and is therefore doubly-symmetric. Figures 7.1 and 7.2 depict the envelope of the roof under the angles of 45° and 225°. These tests exhibit similar behavior, although the formation of conical vortices due to the separation of air flow from the leading roof edge is more visible at the angle of 45° due to the more refined static pressure tap spacing in the upwind corner. Therefore, the doubly-symmetric conditions of the building model were verified and allow the testing range to be reduced to be 0° to 90°.

As discussed in Chapter 6, the minimum C_p increases for the roof surface and top of the parapet wall and decreases for the inner parapet wall surfaces as the height of the parapet increases. To further reduce the number of angles required for evaluation, the test matrix data of Chapter 6 was analyzed in detail. The worst case suction loads were experienced on the roof and top of the parapet at 45° and the inner

parapet wall at 90°. Therefore, each particle will require two BLWT tests for each iteration, one at 45° and one at 90°.

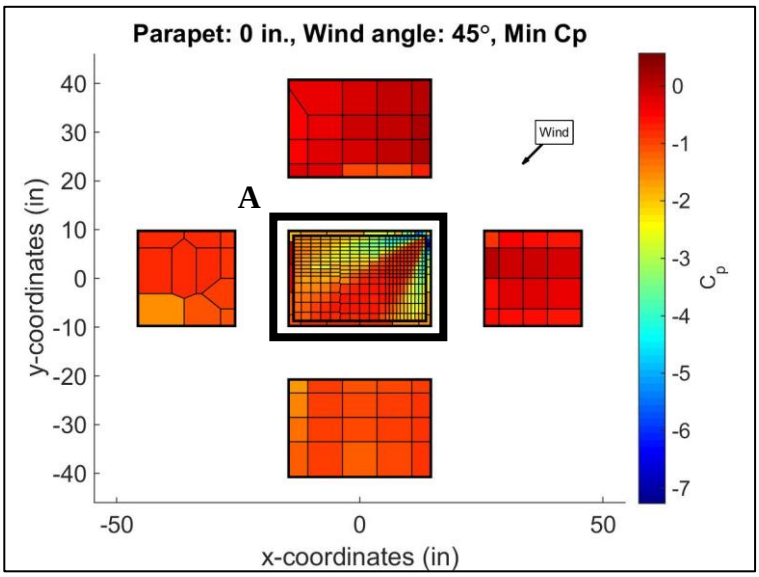

Figure 7.1 Minimum C_p for all surfaces for no parapet at an angle of 0°

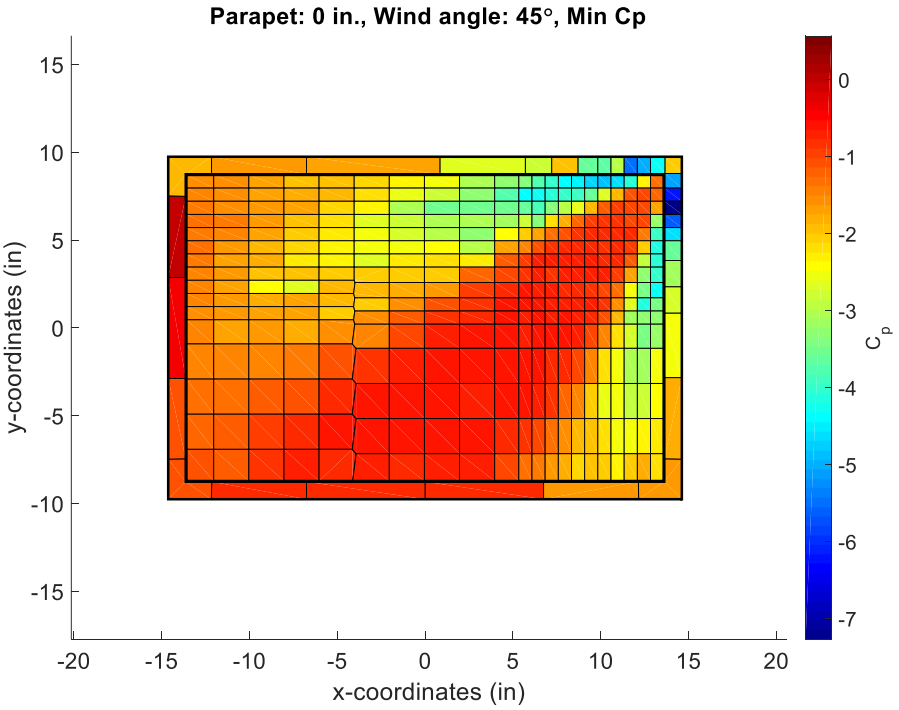

Figure 7.2 Surface A of Figure 7.1

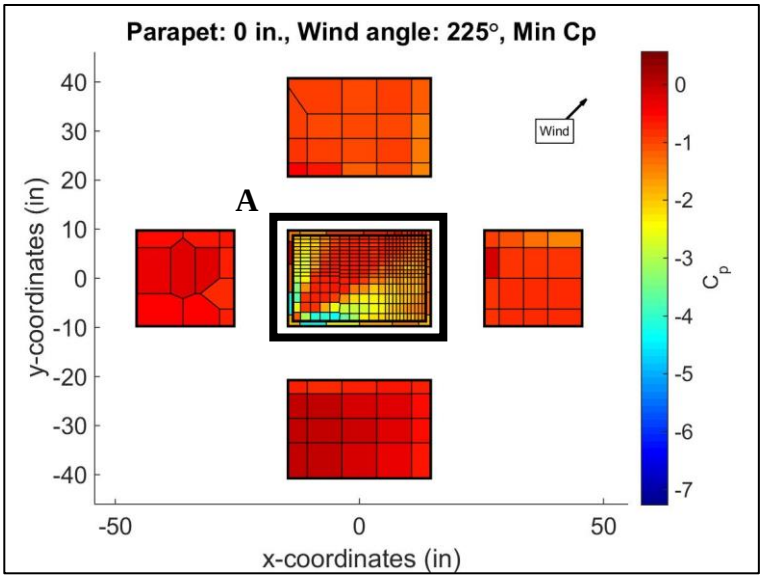

Figure 7.3 Minimum C_p for all surfaces for no parapet at an angle of 225°

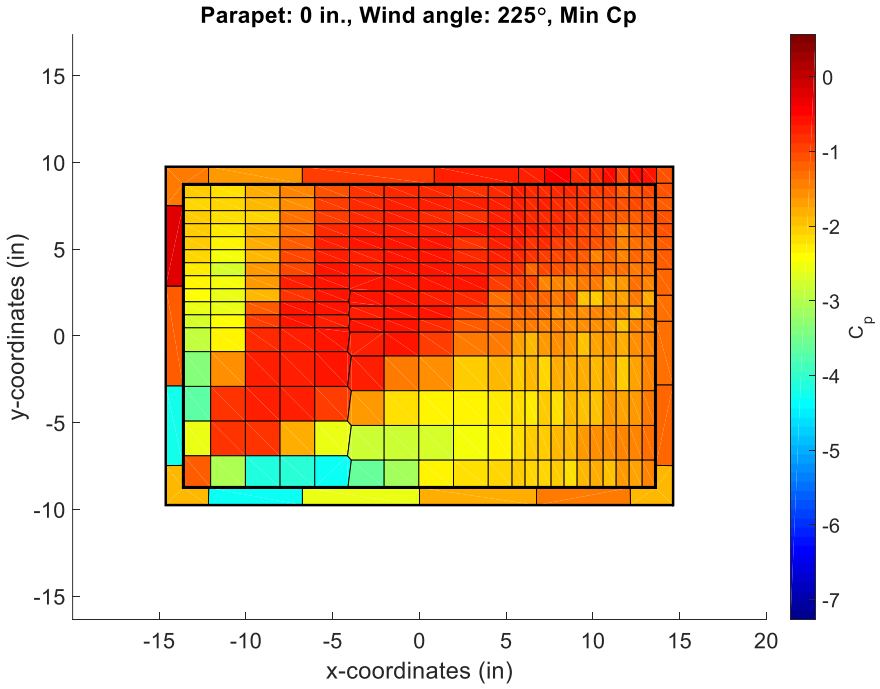

Figure 7.4 Surface A of Figure 7.3

7.2 File Structure

The file structure that was used for the operation of the boundary layer wind tunnel, actuation of the Nanotec linear actuators, and optimization of the parapet

height is diagrammed in Figure 7.5. There were two separate instances of MATLAB R2014b running simultaneously; a master file and a processing file. The processing file was continuously running and was responsible for processing new data while the master file controls the testing and analysis processes.

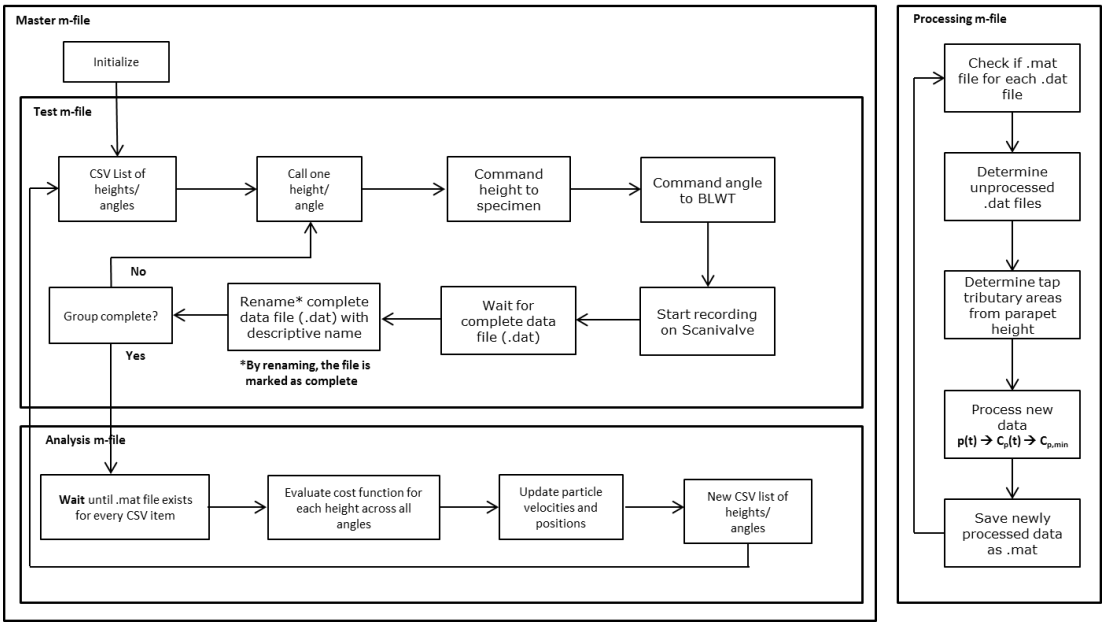

Figure 7.5 Logic diagram for file structure

The details of the BLWT optimization process involving the actuation of the model parapet and the BLWT turntable that occur as a result of the PSO algorithm are outlined in Figure 7.6.

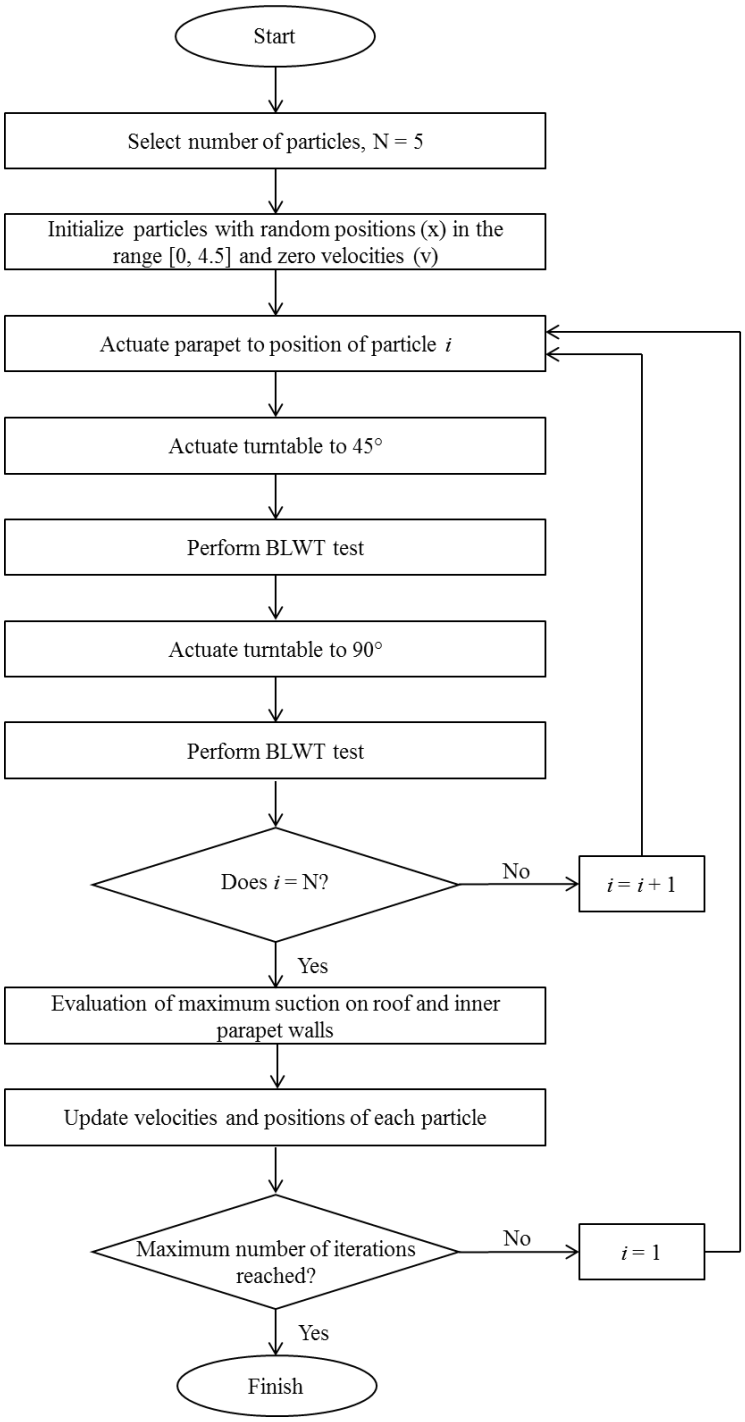

Figure 7.6 BLWT optimization process

7.3 Chapter Summary

The optimization problem setup is presented in this chapter in detail, including the specific objective, constraints, and PSO parameters. The height of the model

parapet is constrained to be between 0 and 4.5 inches. The selection of problem-specific PSO parameters are explained as well. The problem-specific PSO parameters are selected to be $w = c_1 = c_2 = 0.5$. This places an equal weight on all components of the velocity and ensures the particles remain in the feasible design space. The doubly-symmetric conditions of the building model were also verified, and the testing range is to be reduced to be 0° to 90°. The file structure used within MATLAB is presented as well.

Chapter 8: Optimization Results and Analysis

This chapter presents the results for the optimization problem in consideration of the static envelope, including the results and the data analysis.

8.1 Results

A total of 13 design iterations were conducted for the 5 particles within the swarm. To assist in the initial exploration properties of the particles, and considering the experimental runtime required for one full iteration, the position of the particles was initially uniformly distributed across the range of positions. The convergence of the particles towards the optimum height of 2.69 inches is expressed in Figure 8.1. Four of the five particles converge towards the global best cost. The one particle that does not converge is likely due to the particle being equally attracted to both its personal best cost (achieved at iteration 1) and the global best cost. The global best cost for each iteration as well as the particle which obtains this cost is depicted in Figure 8.2. Figures 8.3 and 8.4 depict the envelope plot of the minimum C_p for the optimal solution for 45° and 90° respectively. This illustrates the balance in C_p on the roof and top of the parapet wall at 45° and inner parapet wall surfaces at 90°. This behavior is expected because the roof, inner parapet walls, and top of the parapet were the surfaces of particular interest.

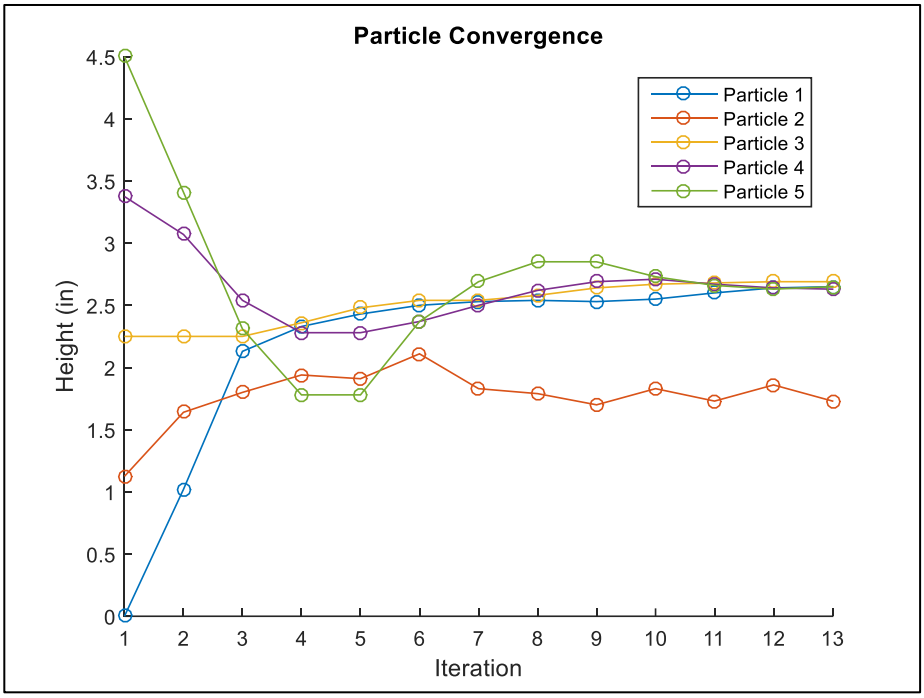

Figure 8.1 Particle convergence over time

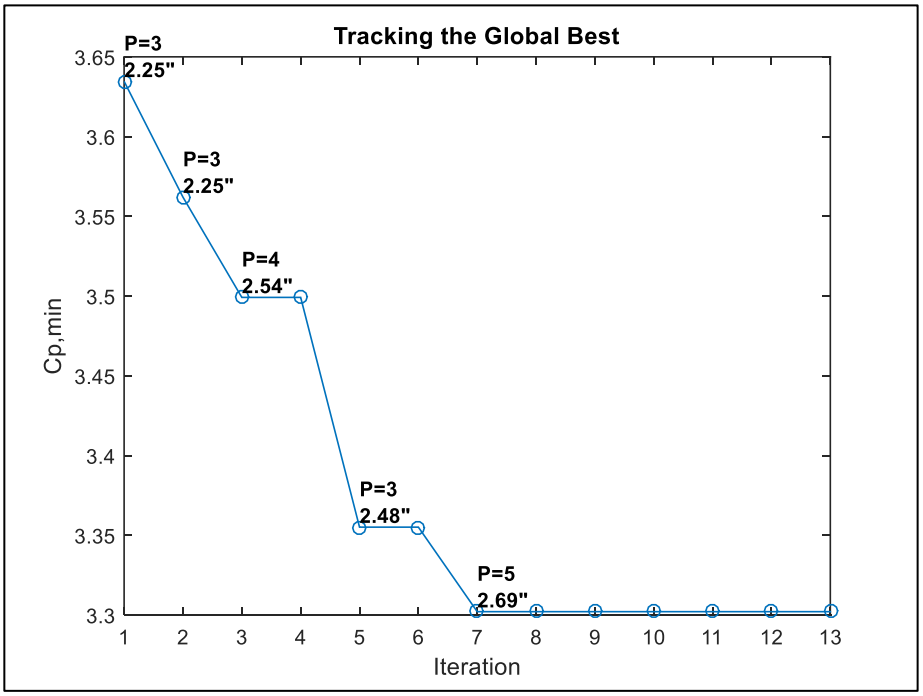

Figure 8.2 Global best cost over time

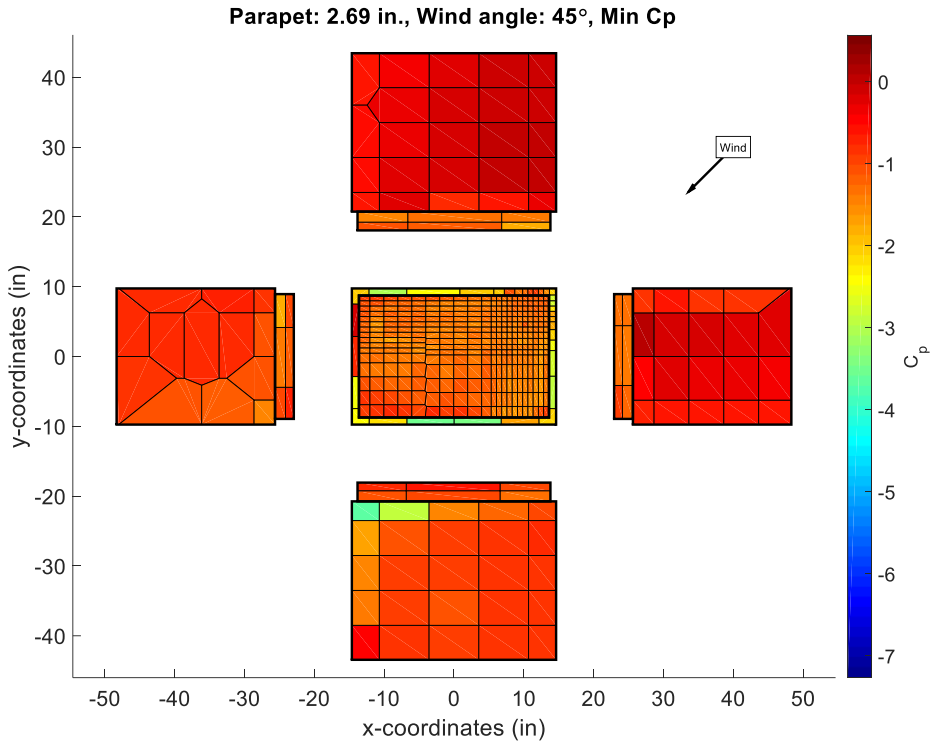

Figure 8.3 Minimum C_p for envelope of optimum solution at 45°

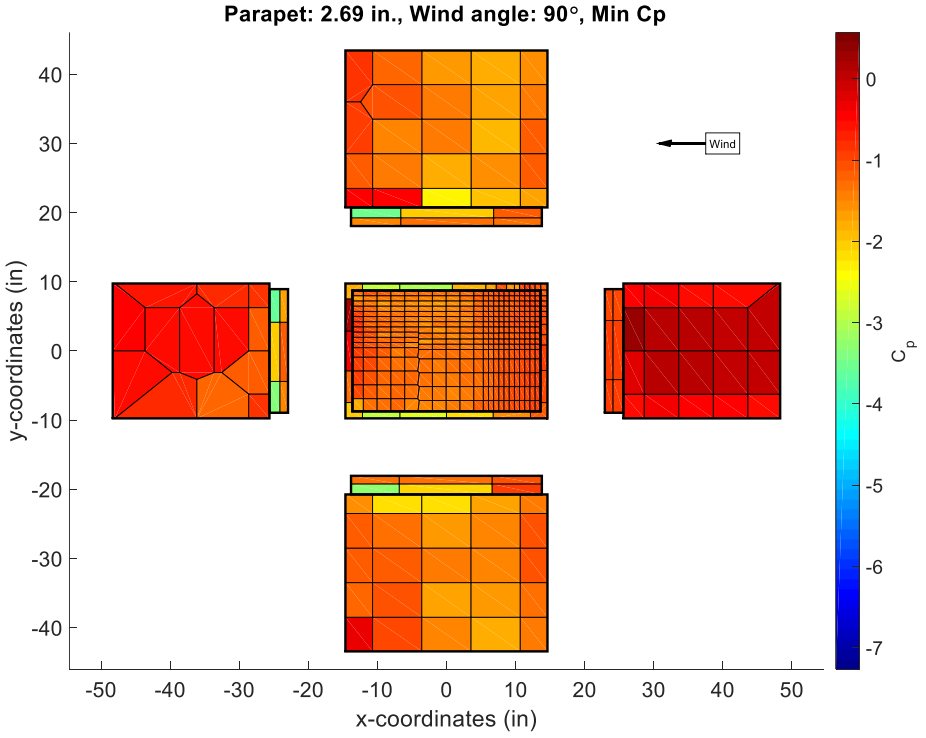

Figure 8.4 Minimum C_p for envelope of optimum solution at 90°

8.2 Data Analysis

These results signify a parapet height that has a full-scale height of 4.035 feet, an otherwise non-intuitive design. This was obtained by minimizing suction on the surfaces of the roof, inner parapet walls, and top of the parapet. Since the inner parapet wall surfaces were considered a part of the objective function, an increased density of taps on the inner parapet walls would prove to be beneficial for future studies. The results obtained are consistent with those from the preliminary test matrix.

According to the Building Code Requirements for Masonry Structures, the height of structural parapets should not exceed 3 times their thickness [27]. These results imply that the optimum parapet height for the given structure upholds this recommendation by the American Concrete Institute, as 4.035 feet is shorter than 4.5 feet.

8.3 Chapter Summary

This chapter presents the particle swarm optimization (PSO) results for the model of a low-rise building with a parapet. For the low-rise building with a parapet, the optimum parapet height in consideration of the static envelope on the roof is investigated. First, the particle position histories are provided to demonstrate their convergence on the global optimum height. The successful convergence of four of the five particles to the same height proves that it is a logical solution to the PSO algorithm and can be considered the optimum parapet height.

Chapter 9: Conclusions and Recommendations

9.1 Conclusions

This thesis investigates the effect of wind on low-rise buildings with parapets for a particular building shape and size. The main goal is to develop a proof-of-concept cyber-physical approach to the optimal design of wind-sensitive structures. The study focuses on the direction of induced pressures on a structure's roof due to the presence of a parapet and determination of the optimum parapet height considering a static pressure envelope.

In terms of structural parapets surrounding a building, ASCE 7-10 does not provide sufficient detail to analyze the influence of varying parapet heights. The results of the preliminary testing for the wind pressure on the inner parapet walls do not fully agree with those expected from the provisions of ASCE 7-10. Therefore, a wind tunnel is used to obtain a better understanding of the behavior of the flow of wind across a structure with a parapet.

After performing preliminary testing to ensure that the model was constructed properly, and that all of the static pressure taps being considered were reading pressure data as expected, particle swarm optimization (PSO) was implemented. Particle swarm optimization allows for the possibility of non-intuitive solutions. In conclusion, the modified PSO algorithm proposed in this thesis proved to be a feasible algorithm, and obtained the result of 2.69 inches, a full-scale height of 4.035 feet for the optimum parapet height of the given structure. Implications are significant for more complex structures where the optimal solution may not be obvious and

cannot be reasonably determined with traditional experimental or computational methods

9.2 Future Studies

Some recommendations for future studies related to this work are:

- The directions of expected wind pressure on the roof and inner parapet wall surfaces are not in agreement with those in ASCE 7-10. The windward parapet wall appears to reduce the positive wall pressure on the leeward parapet wall through shielding. The roof edge along the leeward parapet wall appears to experience positive wind pressure. The behavior of wind over the inner parapet wall and roof surfaces should be investigated with a more refined distribution of static pressure taps.
- In this thesis, the optimum parapet height is determined from the maximum minimum C_p values on the roof, inner parapet walls, and top of the parapet wall. Further studies should focus on optimizing the total weight of the underlying structural frame, to include the cost of the parapet.
- In this thesis, the optimization is for a single objective function. Further studies should focus on multi-objective optimization of structures with parapets through the use of wind tunnel testing.

Bibliography

[1] Pollard, Kelvin M. “Which Types of Disasters Are the Deadliest in the U.S.? The Answer Is Surprising.” *Population Reference Bureau,* Jan. 2011, www.prb.org/Publications/Articles/2011/disasters-by-type.aspx.

[2] “Summary of Natural Hazard Statistics for 2014 in the United States.” *National Weather Service,* 13 May 2016, www.nws.noaa.gov/os/hazstats/sum14.pdf.

[3] “Summary of Natural Hazard Statistics for 2015 in the United States.” *National Weather Service,* 13 May 2016, www.nws.noaa.gov/os/hazstats/sum15.pdf.

[4] *Minimum Design Loads for Buildings and Other Structures*. (2010). Reston, VA: American Society of Civil Engineers.

[5] Kopp, Gregory A., et al. “Wind effects of parapets on low buildings: Part 1. Basic aerodynamics and local loads.” *Journal of Wind Engineering and Industrial Aerodynamics,* vol. 93, no. 11, 10 Oct. 2005, pp. 817–841.

[6] Kopp, Gregory A., et al. “Wind effects of parapets on low buildings: Part 2. Structural loads.” *Journal of Wind Engineering and Industrial Aerodynamics*, vol. 93, no. 11, 10 Oct. 2005, pp. 843–855.

[7] Kopp, Gregory A., et al. “Wind effects of parapets on low buildings: Part 3. Parapet loads.” *Journal of Wind Engineering and Industrial Aerodynamics,* vol. 93, no. 11, 10 Oct. 2005, pp. 857–872.

[8] Kopp, Gregory A., et al. “Wind effects of parapets on low buildings: Part 4. Mitigation of corner loads with alternative geometries.” *Journal of Wind Engineering and Industrial Aerodynamics,* vol. 93, no. 11, 10 Oct. 2005, pp. 873–888.

[9] Robinson, Jacob, and Yahya Rahmat-Samii. "Particle Swarm Optimization in Electromagnetics." *IEEE Transactions on Antennas and Propagation* 52.2 (2004): 397-407. Web.

[10] Talbi, El-Ghazali. *Metaheuristics: From Design to Implementation*. Hoboken (NJ): John Wiley & Sons, 2009. Print.

[11] Perez, R. E., & Behdinan, K. (2007). Particle Swarm Optimization in Structural Design. *Swarm Intelligence: Focus on Ant and Particle Swarm Optimization*, 373-377.

[12] Shi, Y., and R. Eberhart. “A Modified Particle Swarm Optimizer.” *1998 IEEE International Conference on Evolutionary Computation Proceedings. IEEE World Congress on Computational Intelligence (Cat. No.98TH8360),* pp. 69–73.

[13] Fourie, P.C., and A.A. Groenwold. “The particle swarm optimization algorithm in size and shape optimization.” *Structural and Multidisciplinary Optimization*, vol. 23, no. 4, Jan. 2002, pp. 259–267.

[14] Kennedy, J., and Eberhart, R. C., “Particle Swarm Optimization,” Proceedings of the 1995 IEEE International Conference on Neural Networks, Vol. 4, Inst. of Electrical and Electronics Engineers, Piscataway, NJ, 1995, pp. 1942–1948.

[15] Shi, Yuhui, and Russell C. Eberhart. “Parameter selection in particle swarm optimization.” *Lecture Notes in Computer Science Evolutionary Programming VII*, 1998, pp. 591–600.

[16] Venter, Gerhard, and Jaroslaw Sobieszczanski-Sobieski. “Particle Swarm Optimization.” *AIAA Journal*, vol. 41, no. 8, Aug. 2003, pp. 1583–1589.

[17] He, S., et al. “An improved particle swarm optimizer for mechanical design optimization problems.” *Engineering Optimization*, vol. 36, no. 5, 2004, pp. 585–605.

[18] Stathopoulos, T., et al. “Wind loads on parapets.” *Journal of Wind Engineering and Industrial Aerodynamics*, vol. 90, no. 4-5, 2002, pp. 503–514.

[19] Kind, R. J. “Worst suctions near edges of flat rooftops with parapets.” *Journal of Wind Engineering and Industrial Aerodynamics*, vol. 31, no. 2-3, Dec. 1988, pp. 251–264.

[20] Pindado, S., and J. Meseguer. “Wind tunnel study on the influence of different parapets on the roof pressure distribution of low-Rise buildings.” *Journal of Wind Engineering and Industrial Aerodynamics*, vol. 91, no. 9, 2003, pp. 1133–1139.

[21] MATLAB version 8.4.0 Natick, Massachusetts: The MathWorks Inc., 2014.

[22] American Institute of Steel Construction, Manual of Steel Construction, 14th Edition. Chicago: AISC, 2010.

[23] Li, L. J., et al. “A heuristic particle swarm optimizer for optimization of pin connected structures.” *Computers & Structures*, vol. 85, no. 7-8, 18 Jan. 2007, pp. 340–349.

[24] Schmit, L. A., and B. Farshi. “Some approximation concepts for structural synthesis.” *AIAA Journal*, vol. 12, no. 5, 1974, pp. 692–699.

[25] Rizzi, Paulo. “Optimization Of Multi-Constrained Structures Based On Optimality Criteria?” *17th Structures, Structural Dynamics, and Materials Conference*, 1 Jan. 1976, pp. 448–462.

[26] Lee, Kang Seok, and Zong Woo Geem. “A new structural optimization method based on the harmony search algorithm.” *Computers & Structures*, vol. 82, no. 9-10, Apr. 2004, pp. 781–798.

[27] *Building code requirements and specification for masonry structures: containing Building code requirements for masonry structures (TMS 402-11/ACI 530-11 / ASCE 5-11), Specification for mason structures (TMS 602-11 / ACI 530.1-11 / ASCE 6-11) and companion commentaries / developed by the Masonry Standards Joint Committee (MSJC)*. Boulder, Co., The Masonry Society, 2011.